Molecular and Cellular Neuroscience 120 (2022) 103731

Contents lists available at ScienceDirect

Molecular and Cellular Neuroscience

journal homepage: www.elsevier.com/locate/ymcne

Elevated ATG13 in serum of patients with ME/CFS stimulates oxidative stress response in microglial cells via activation of receptor for advanced glycation end products (RAGE)

Gunnar Gottschalk [a,b], Daniel Peterson [a], Konstance Knox [c], Marco Maynard [b], Ryan J. Whelan [b], Avik Roy [a,b,*]

[a] Simmaron Research Institute, 948 Incline Way, Incline Village, NV 89451, United States of America
[b] Simmaron R&D lab, Technology Innovation Center, 10437 W Innovation Drive, Wauwatosa, WI 53226, United States of America
[c] Coppe Laboratories, W229N1870 Westwood Dr, Waukesha, WI 53186., United States of America

ARTICLE INFO

Keywords:
ME/CFS
Microglia: RAGE
ATG13
ROS
NO
Autophagy

ABSTRACT

Myalgic Encephalomyelitis, also known as Chronic Fatigue Syndrome (ME/CFS), is a multisystem illness characterized by extreme muscle fatigue associated with pain, neurocognitive impairment, and chronic inflammation. Despite intense investigation, the molecular mechanism of this disease is still unknown. Here we demonstrate that autophagy-related protein ATG13 is strongly upregulated in the serum of ME/CFS patients, indicative of impairment in the metabolic events of autophagy. A Thioflavin T-based protein aggregation assay, array screening for autophagy-related factors, densitometric analyses, and confirmation with ELISA revealed that the level of ATG13 was strongly elevated in serum samples of ME/CFS patients compared to age-matched controls. Moreover, our microglia-based oxidative stress response experiments indicated that serum samples of ME/CFS patients evoke the production of reactive oxygen species (ROS) and nitric oxide in human HMC3 microglial cells, whereas neutralization of ATG13 strongly diminishes the production of ROS and NO, suggesting that ATG13 plays a role in the observed stress response in microglial cells. Finally, an in vitro ligand binding assay provided evidence that ATG13 employs the Receptor for Advanced Glycation End-products (RAGE) to stimulate ROS in microglial cells. Collectively, our results suggest that an impairment of autophagy following the release of ATG13 into serum could be a pathological signal in ME/CFS.

1. Introduction

Myalgic Encephalomyelitis/Chronic Fatigue Syndrome (ME/CFS) is a chronic inflammatory disease characterized by muscle fatigue, pain, dizziness, and brain fog. Despite intense investigation, the molecular mechanism of this disease is not yet understood. When one group believes that the acute viral infection (Buchwald et al., 1992; Rasa et al., 2018), viral reactivation (Josephs et al., 1991), and resultant dysregulation of innate immune response (Mensah et al., 2017; Milivojevic et al., 2020) could be the primary mechanism of chronic inflammation in ME/CFS, another group emphasizes that the biochemical deficit of mitochondrial energy metabolism (Armstrong et al., 2015; Filler et al., 2014; Morris and Maes, 2014; Tomas et al., 2020) and impairment of ion transport mechanism through β2 adrenergic receptors in skeletal muscle (Wirth and Scheibenbogen, 2021) are more direct mechanisms for muscle fatigue. Recently, a severe depolarization of mitochondrial membrane potential that could affect mitochondrial function was observed in immune cells such as T cells (Mandarano et al., 2020) and NK cells (Silvestre et al., 2019) suggesting that altered mitochondrial metabolism could be responsible for immune dysregulation in ME/CFS patients. Therefore, defective mitochondrial energy metabolism could be a critical molecular mechanism for both metabolic and

Abbreviations: ME/CFS, myalgic encephalomyelitis and chronic fatigue syndrome; *ROS*, reactive oxygen species; *RAGE*, receptor for advanced glycation end products; ATG13, autophagy related protein 13. *NO* = Nitric Oxide (NO in a soluble form); *mTOR*, mammalian target of rapamycin; *ME*, myalgic encephalomyelitis; *HC*, healthy control; *r.t.*, room temperature; iNOS, inducible nitric oxide synthase.

* Corresponding author at: Simmaron Research Institute, Technology Innovation Center, 10437 W Innovation Drive, Suite # 325, Wauwatosa, WI 53226, United States of America.
E-mail address: aroy@simmaron.com (A. Roy).

https://doi.org/10.1016/j.mcn.2022.103731
Received 28 December 2021; Received in revised form 13 April 2022; Accepted 17 April 2022
Available online 26 April 2022
1044-7431/Published by Elsevier Inc.

immunological dysregulation in ME/CFS patients. However, it is not known if autophagy, the biochemical process that regulates mitochondrial quality control process, is impaired in ME/CFS patients.

Autophagy is a biochemical process in which metabolically inactive proteins and defective mitochondria undergo hydrolysis in lysosomes (Mizushima, 2007; Rabinowitz and White, 2010; Roy, 2016). In fact, autophagy selectively targets depolarized mitochondria (Okamoto and Kondo-Okamoto, 2012), maintains mitochondrial quality control mechanism, and regulates mitochondrial homeostasis (Evans and Holzbaur, 2020). During that process, dysfunctional cellular components including defective mitochondria are enclosed in vesicular structures known as "autophagosomes" and then fused with lysosomes for subsequent hydrolytic degradation. Formation of autophagosomes is a complex process guided with synchronized actions of multiple proteins. Proteins encoded by the Autophagy-related Gene (ATG) family (Mizushima, 2020; Noda and Fujioka, 2015), the LC3/GABARAP family (Tanida et al., 2008), p62 (Moscat and Diaz-Meco, 2009), beclin-1 (He and Levine, 2010), and VPS-34 (Jaber et al., 2012) primarily regulate the initiation, maturation, and lysosomal fusion of autophagosomes. On the other hand, cathepsin D (Benes et al., 2008), cathepsin B (Mort and Buttle, 1997), LAMP-1 (Eskelinen, 2006), and 50 different acid hydrolases (Saftig, 2006) are lysosome-resident factors that directly participate in the degradation of these inactive components. Accordingly, impaired mechanisms of autophagy (Komatsu et al., 2006), coupled with lysosomal dysfunction (Zhang et al., 2021) are responsible for the cellular accumulation of depolarized mitochondria and aberrant protein aggregates. Together, these factors are considered to be major contributing elements in the pathogenesis of many disorders, including Parkinson's disease (PD) (Ahmed et al., 2012; Cerri and Blandini, 2019; Lane et al., 2017), Alzheimer's disease (AD) (Kragh et al., 2012; Nassif and Hetz, 2012), stroke (Liu et al., 2010; Luo et al., 2013), and cancers (Mathew et al., 2007; White, 2012). However, autophagy impairment has not been studied in ME/CFS. Because autophagy impairment contributes to the pathogenesis of many chronic inflammatory and cognitive disorders, we considered it important to examine this phenomenon in ME/CFS, given that inflammation and cognitive problems are well known to occur in the disease (Anon, 2015).

Altered levels of autophagy-related proteins in plasma have been directly correlated with the pathogenesis of many metabolic disorders. Higher levels of lysosomal membrane protein LAMP-1 were detected in lysosomal storage diseases (Meikle et al., 1997; Ranierri et al., 1999). One report found that plasma ATG5 level was elevated in Alzheimer's disease (AD) patients (Cho et al., 2019), while another observed lower ATG5 and mitophagy in serum from patients exhibiting mild cognitive impairment, vascular dementia, and Alzheimer's disease (Castellazzi et al., 2019). Beclin-1 and LC3 are observed in the serum in patients with acute ischemic stroke (Li et al., 2015). Levels of autophagic markers might be associated with coronary total occlusion and childhood cerebral palsy (Demircan et al., 2018; Xu et al., 2017). Upregulation of α-syn was demonstrated in plasma of PD patients (Bougea et al., 2019). However, it is not known if the levels of these autophagy markers are also altered in ME/CFS.

To explore the molecular regulation of autophagy proteins in ME/CFS patients, double-blinded antibody array analyses of 20 autophagy-related proteins were performed in the serum samples of two case-control subjects that demonstrated strong elevation of ATG13. The result was further validated with ELISA analyses in ME/CFS patients ($n = 10$). Moreover, our in vitro cell culture study clearly demonstrated that the serum-derived ATG13 was metabolically toxic, resulting in an induction of the oxidative stress response and nitric oxide (NO) production in HMC3 human microglial cells via activation of RAGE.

2. Materials and methods

2.1. Reagents

Human autophagy array kit (Cat # AAH-ATG-1-4) was purchased from RayBiotech (Georgia, USA). Human p62/SQSTM1 ELISA kit (Cat# MBS3801969), Autophagy protein 5 (ATG5) ELISA kit (Cat# MBS7209535), ATG13 ELISA kit (Cat# MBS7239399), LC3A ELISA kit (Cat# MBS7253712), and α-syn ELISA kit (Cat # MBS161176) were purchased from My BioSource (San Diego, Southern California, USA). IRDye800-conjugated anti-rabbit and anti-mouse antibodies was obtained from LI-COR Biosciences (Lincoln, NE). IRDye800-conjugated streptavidin (Cat# 926-32230) was also purchased from LI-COR for the endpoint detection of human autophagy array in Odyssey SA infrared imager. Thioflavin T (Cat # T3516) and ammonium sulphate (Cat # A4418) came from Sigma. HMC3 human transformed microglial cell lines (ATCC® CRL-3304™) was provided by the American Type Culture Collection and maintained with complete DMEM media supplemented with 10% FBS (Lot # 2346974RP; Gibco), 2 mM L-glutamine (Ref# 25030-081: Gibco) and antibiotic-antimycotic compounds. All media supplements were purchased from ThermoFisher scientific. CO_2 gas was supplied by Sheeley Service INC (Milwaukee, WI).

2.2. Acquisition of samples and handling patient record

Blood samples and questionnaire data were previously collected under the supervision of Dr. Daniel Peterson (Sierra Internal Medicine, Incline Village, NV) (Western IRB) #20201812. Blood samples were centrifuged, and serum samples were aliquoted and then immediately frozen at −80 °C. Each sample was given a unique identification number and recorded both in a notebook and Microsoft Excel with date and signature per the IRB-approved protocol. Samples were then delivered to our research facility in Wisconsin on dry ice overnight. Upon receipt, samples were processed and assayed immediately. Questionnaire and de-identified clinical data are stored in a secure, limited access Redcap sever database managed by the Research Staff and Clinical Fellow at Sierra Internal Medicine. Patient records were maintained with was privacy policy guidelines set by Sierra Internal Medicine.

2.3. Antibody array

The RayBio ® C-series Human Autophagy Array was performed as described in THE manufacturer's protocol. The array membrane was engraved with 20 autophagy-related proteins in duplicate in 8 × 8 format. Briefly, each membrane was soaked with blocking buffer for 1 h, incubated with 1:5 diluted serum samples (1.4 mg protein as measured with Bradford protein detection method) for 5 h at 37 °C, washed 5 times with 1× wash buffer, incubated with biotin-conjugated secondary antibody for 2 h at 37 °C followed by wash (5×) and detection with IRDye800-conjugated streptavidin at Licor Odyssey Sa infrared scanner. All necessary reagents and antibodies were supplied with the kit except IRDye800-conjugated streptavidin because the application of streptavidin conjugate was devised for the detection of membrane in Sa scanner. The scanning process was done at resolution of 200 μm with focus offset at 3.0 mm. The density of individual proteins was measured in ImageJ software, subtracted from blank, normalized with the positive control, and then plotted at GraphPad Prism 8 software.

2.4. Colorimetric competitive ELISA

Colorimetric ELISA was performed as per the manufacturer's protocol supplied with kits from MyBioSource INC. (San Diego, CA). Briefly, serum samples were diluted with assay diluent at a dilution of 1:4 (v/v) and incubated on a 96 well strip plate with wells pre-coated with capture antibodies followed by 30 min incubation at room temperature (r.t) shaking. Then biotinylated assay conjugate was added and incubated for

24 h at 4 °C. Subsequently, each well was aspirated, washed 3 times, and then HRP-conjugated detection antibody was added, followed by incubation for 2 h at r.t., shaking. After that, each well was aspirated, and color was developed with TMB substrate. Optical density was measured at 450 nm excitation filter in a Victor X3 multi-channel plate reader. According to the competitive ELISA, more color indicates less abundance of the target in serum, resulting a non-linear regression standard curve with negative slope. The optical density (Y) was converted to absolute amount (X) with following equation Y = Bottom + (Top-Bottom) / [1 + (X/IC50)] using GraphPad Prism 8.

2.5. Near infra-red ELISA

After overnight incubation with sample in a pre-coated 96 well plate probed with biotinylated secondary antibodies for 2 h. Biotin conjugation of polyclonal anti-ATG13 (Host; Rabbit; Cat# 18258-1-AP; Proteintech), ATG5 (Host; Rabbit; Cat# 10181-2-AP; Proteintech), and LC3a antibodies (Host; Rabbit; Cat# 18722-1-AP; Proteintech) were performed with SiteClick™ Biotin Antibody Labeling Kit purchased from ThermoFisher (Cat # S20033). After that, IRDye800-conjugated STREPTAVIDIN was probed for 2 h, imaged in a LI-COR Odyssey SA scanner, and finally analyzed with the integrated density measurement tool in the Odyssey Sa imager.

2.6. Fluorometric Thioflavin T assay

Serum samples were centrifuged at 800 rpm to remove the macromolecular impurities Protein concentration was measured by the BCA method. 5 μL serum (~200 μg of protein) was then mixed with 4 M ammonium sulfate (55 mg in 1 mL ddH_20) solution and then plated in a 96 well plate (reaction volume is 100 μL). Diluted (1:5 in 1× PBS) Thioflavin T (ThT) solution (stock: 8 mg of ThT in 1× PBS; kept in dark at 4 °C) was dispensed via an auto-dispenser and plate reading was performed immediately in a Victor X3 fluorescent plate-reader with 450 nm excitation and 486 nm emission wavelengths for 90 min at 3 min intervals.

2.7. ATG13 neutralization and siRNA knock-down experiments

100 μL serum samples were diluted with 100 μL sterile DMEM supplemented with protease inhibitors [2 μg/mL aprotinin (Cat # 78432; Thermofisher), 1 μg/mL leupeptin (Cat# 78435; Thermofisher), and 25 μg/mL PMSF (Cat# 36978; Thermofisher)] and then added on a 96-well plate precoated with ATG13 capture antibody. After 30 mins of incubation at 37 °C, the media was carefully harvested from the top and used for subsequent experiments. The neutralization of ATG13 was confirmed with ELISA analyses in serum before and after neutralization. For siRNA experiments, HMC3 microglial cells (80% confluent) were kept serum-free and then transfected with 0.5 μg siRNA via lipofectamine 3000 (Invitrogen; lot # 2381886). After 4 h, 20% FBS-containing DMEM media (no antibiotic) was added. After another 18 h, cells were infused with DCFDA and then measured for ROS after 30 min.

2.8. Microglial cell culture, fluorometric ROS assay, and microscopy

HMC3 human embryonic microglial cells were thawed from liquid nitrogen, immediately poured in 15 mL of fresh complete DMEM/F12 media kept in a 75 mm flat surface sterile tissue culture flask, and then placed inside a temperature-controlled CO_2 incubator (37 °C/5% CO_2). After 2 days, media was replaced with 15 mL of fresh DMEM/F12 complete media. After 10 days, when cells were confluently growing, passaging was performed. After 3 passages, cells were harvested and plated in a 96-well-plate for ROS fluorometric and kinetic study. Cells were allowed to grow to 75–80% confluency, incubated with DCFDA probe (Cat# ab113851; Abcam) for 45 mins at 37 °C in dark, media were replaced with 100 μL (1:2 dilution = 50 μL serum +50 μL media) serum-supplemented media, and then left for different time periods, starting from 30 mins to 2 h. At the end of an incubation period, media was aspirated and then imaged under the FITC channel of a Hund fluorescence microscope. For kinetic assay, media was not aspirated. Media-embedded cells were kept in a VictorX3 fluorimeter at different time points and reading was recorded at 485 nm/53 m nm (Ex/Em) fluorescence reading protocol.

2.9. Nitric oxide assay

Serum-induced production of nitric oxide (NO) in HMC3 microglial cells was evaluated via fluorimetric assay [Cat # 780051; Cayman chemical]. The final products of NO are NO (NO_2^-) and nitrate (NO_3^-). The fluorimetric assay quantified total NO production as a sum of both NO_2^- and NO_3^-. HMC3 microglial cells (50,000 cells/well in a 96-well plate) were treated with 25 μM of L-NIL (iNOS inhibitor) [Cat # 80310; Cayman Chemical] under serum free condition for 2 h (Roy et al., 2006) followed by the treatment with ME serum (1:2 dilution). After another 22 h, supernatants were harvested, diluted 4-times with assay buffer, and then mixed with enzyme cofactor and nitrate reductase enzymes. After 1 h of incubation, 10 μL of 2,3-diaminonapthalene (DAN) was added in each well, incubated for 10 min, and then added with NaOH. Plate reading was performed in Victor X3 plate reader [Ex:/Em:355 nm/460 nm].

2.10. Binding and neutralization assay of ATG13 with RAGE

Biotinylated RAGE extracellular domain was purchased from Aviscera Bioscience (Cat # 00112–02-50B) and recombinant carrier-free ATG13 protein (Cat # ab127606) was purchased from Abcam. ATG13 protein was suspended in carbonate coating buffer at a concentration range from 0 to 10 ng and then plated in a 96 well plate overnight at 4 °C. The next day, the remaining buffer was aspirated and then the plates were incubated with Li-Cor blocking buffer for 30 mins. Subsequently, 2.5 ng of biotinylated-RAGE was added per well and incubated at 37 °C for 1 h. After 2× washing with 1× PBS (2 mins each), 1:1000 diluted IRDye800-conjugated streptavidin was added to each well, incubated for 1 h at r.t., washed with 1× PBS three times, and then imaged in a Li-Cor Odyssey Sa at an 800 nm wavelength (resolution 300 dpi and focus offset 7). In a neutralization experiment, 2.5 ng of biotinylated RAGE was incubated with increasing doses of RAGE neutralization antibody and immediately added in ATG13 coated well. Competitive inhibition of binding was evaluated with IRDye800-tagged streptavidin.

2.11. In silico homology modeling to dock ATG13 in RAGE extracellular domain

PDB structures of ATG13 and RAGE were derived from structures with PDB ID 4YK8 and 2M1K, respectively, followed by docking in the PyDock server. The resultant structure with the most stable energy score was selected and displayed in Chimera software. Predicted H-bonds were derived from the intra-molecular H-bond prediction tool of Chimera.

2.12. Double blinding and statistical analysis

All assays were performed with a double-blinded strategy, in which researcher #1 (AR) was blinded by researcher # 2 (KK) with regard to sample identification. Samples were tagged with a different color tag by KK and given to AR. KK was not aware of disease status of the subject (blinding #2). The unique color code was decoded once the assay completed, and the result was disclosed in the presence of both researchers, consultant, and physician. Finally, the data was plotted in GraphPad Prism 8 software and significance of mean was tested with an unpaired *t*-test at 95% significance interval and $p < 0.05$.

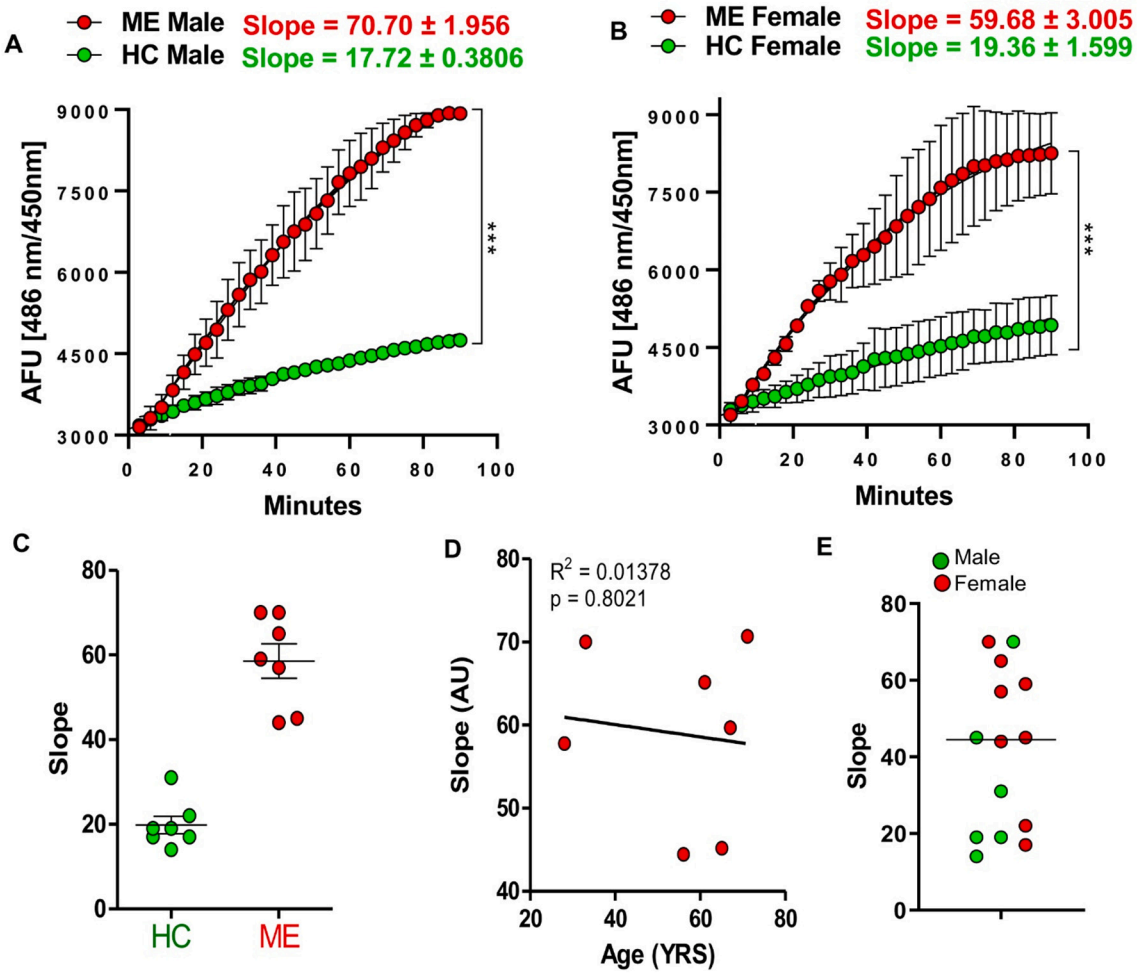

Fig. 1. Thioflavin T assay to measure the protein aggregation tendency of serum proteins. Two-hundred μg protein containing serum samples were assayed for a Thioflavin T(ThT)-based protein aggregation assay. (A) 74-year–old healthy control (HC) male (green) versus 71 years old male ME/CFS patient (ME) (red), (B) 68-year-old HC female versus 67-year-old ME/CFS. The equation for the one-phase saturation non-liner fitted curve is $Y = Y0 + (Plateau - Y0) \times [1 - e^{-K*time}]$. Y0 = Y value when time is 0 min. Plateau is the Y value at infinite times, expressed in the same units as Y. K is the rate constant, expressed in reciprocal of the X axis time unit. ThT Fluorescence absorbance [486/450 nm] was measured from 0 to 90 mins at 3 min of interval after ThT addition through autoinjector. Results are mean ± SD of three independent experiments Comparison of slope values between healthy controls (green) and patients (red). (C) Slope value of ThT based protein aggregation curve for $n = 7$ HC and n⎓7 ME patients (two-tailed unpaired t-test; $t = 8.445$, df = 12; $p < 0.0001$). (D) No significant correlation between protein aggregation slope and age as indicated with r2 = 0.01378 and $p = 0.8021$ ($n = 7$). (G) A dotted bar graph represents that slope value of (55% female and 14% male are higher than median line. Results were confirmed after three independent experiments. (For interpretation of the references to color in this figure legend, the reader is referred to the web version of this article.)

2.13. Sample size determination

For 99% confidence interval and 0.05 significance, our sample size calculation is $n = \frac{z^2 \times p\ (1-p)}{\varepsilon^2} = \frac{1.28^2 \times 0.99\ (1-0.99)}{0.05^2} = 7$. Z is the z score, which is 1.28 for power 0.8; p is the population proportion. For 99% confidence interval, p will be 0.99; ε is the margin of error = 0.05. Therefore, throughout the study we selected at least $n = 7$ per group when comparing results between HC and ME groups.

3. Results

3.1. Clinical history of ME/CFS subjects displaying significant muscle and cognitive impairments

We first performed a pilot study with two age-matched case-control pairs and then validated the findings with 7 other pairs matched by age, gender, ethnicity, and geographical location. Initially, we characterized a serum sample of a 71-year- old white male ME/CFS patient. In 1988, when the subject was 40 years old, he was initially diagnosed with acute flu-like symptom. The disease eventually progressed with severe symptomology of sore throat, acute joint pain, swollen cervical lymph nodes, mental fog, memory impairment, extreme dizziness, and severe fatigue, leaving the patient bedridden 90% of the time. Although the underlying cause of these symptoms was not determined, subsequent antigen testing detected positive titers for EBV, HSV1, and CMV infection. In 1991, the patient was admitted to a clinic in Incline Village, Nevada, along with a cluster of patients with similar clinical symptoms. Single-photon emission computerized tomography (SPECT) scan imaging analyses revealed inflammation of the brain with bilateral hypoperfusion.

Another patient in our pilot study is a 67-year-old female who had similar initial flu-like symptoms in 1988, which rapidly progressed to severe sinus infection with methicillin-resistant staphylococcus aureus (MRSA) infection. Eventually the patient received 6 turbinate surgeries. Although the subject did not have sinus problems prior to the flu-like illness, she now has a history of depression, severe difficulty in sleeping (specifically, staying asleep) and experiences fatigue, pain (general), irritable bowel syndrome, severe memory impairment, and

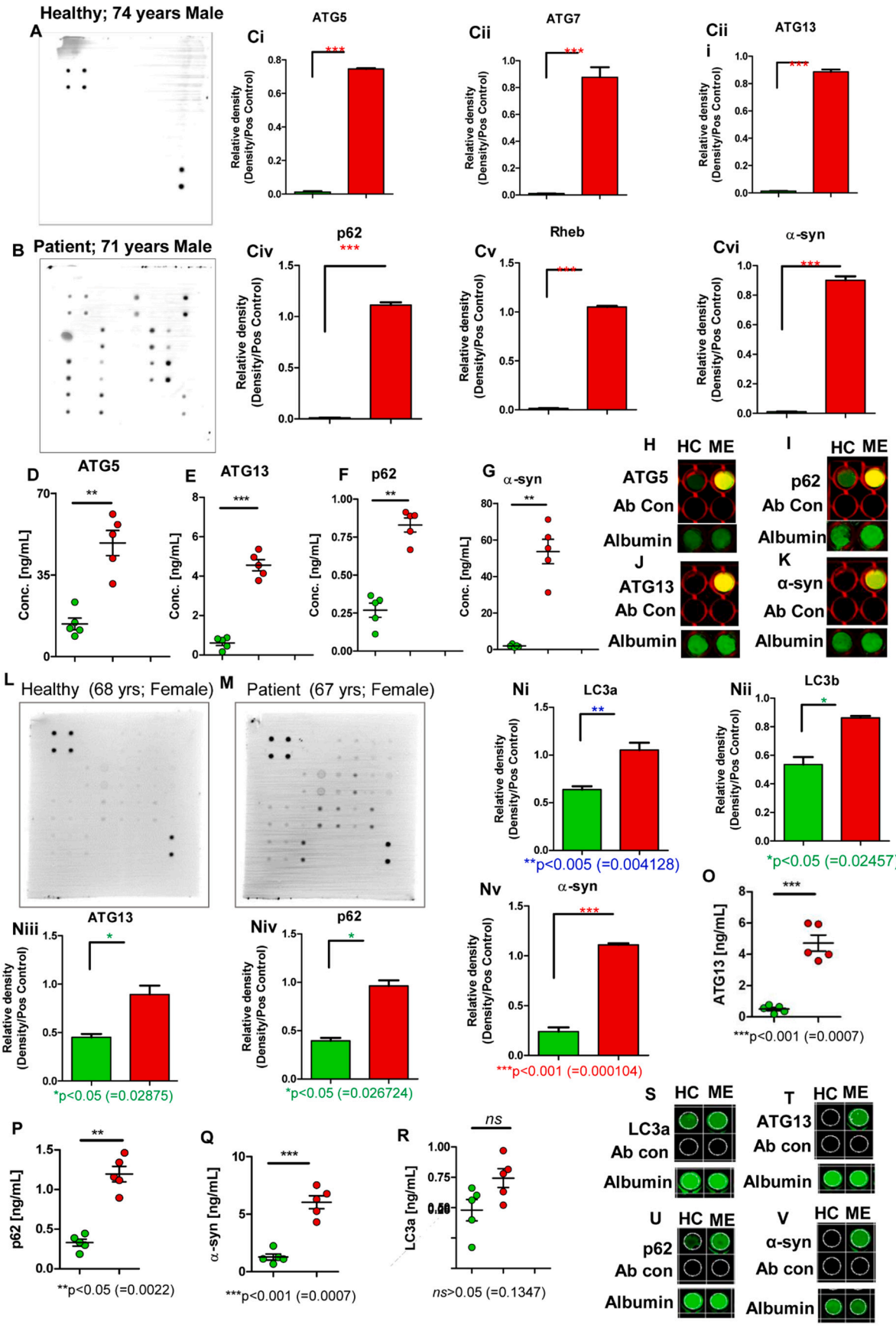

(caption on next page)

Fig. 2. Upregulation of autophagy markers in serum samples of ME/CFS patients: Two case-control pairs. Serum samples of (A) 74-year-old healthy male and (B) 71-years-old male patient were assayed on an antibody array of autophagy biomarkers (RayBiotech; Cat # AAH-ATG-1-4). (Ci-Cvi) Densitometric analyses display strong upregulations of autophagic markers. Dot intensities of (Ci) ATG5 [$***p < 0.005$(=0.000472)], (Cii) ATG7 [$***p < 0.005$(=0.00239), (Ciii) ATG13 [$***p < 0.005$ (=0.00109)], (Civ) p62 [$***p < 0.005$(=0.000293)], (Cv) Rheb [$***p < 0.005$(=0.00334)], and (Cvi) α-syn [$***p < 0.005$(=0.00172)] were measured in ImageJ software (NIH, USA) after subtraction with blank followed by normalization with positive control. Results were mean ± SD and confirmed after three independent experiments. ELISA analyses of (D) ATG5 ($**p < 0.001$), (E) ATG13 ($***p < 0.0001$), (F) p62 ($**p < 0.001$), and (G) α-syn ($**p < 0.001$) were performed in healthy (green) and patient (red). Results were confirmed and considered to be significant after 5 independent experiments and indicated with 5 dots in a dotted histogram. Near -infrared ELISA assay for (H) ATG5, (I) ATG13, (J) p62, (K) α-syn. A paired *t*-test was done to assess the significance of mean. An antibody control was performed by omitting sample addition and then probing each well with only the 2° antibody. Albumin was run for both samples as a loading control. Similarly, an antibody array of autophagy markers in serum samples of (L) 68-year-old HC female and (M) 67-year-old female ME/CFS case followed by densitometric analyses of (Ni) LC3a, (Nii) LC3b, (Niii) ATG13, (Niv) p62, and (Nv) α-syn. Signal intensities were measured in ImageJ software, subtracted from blank, normalized with positive control, and then plotted as a histogram in GraphPad Prism 8 software. Results are mean ± SD of three different experiments. Significance of mean was tested by unpaired *t*-test with *p* value given underneath. Quantitative ELISA analyses for (O) ATG13, (P) p62, (Q) α-syn, and (R) LC3a were performed in serum samples of HC (green) and ME (red) (paired t-test). Near-infrared ELISA analyses for (S) LC3a, (T) ATG13, (U) p62, and (V) α-syn. (For interpretation of the references to color in this figure legend, the reader is referred to the web version of this article.)

major brain fog. Recently the patient has experienced extremely high blood pressure, with no noted cardiac dysfunction.

We matched the first two cases with appropriate age- and sex-matched healthy controls. We included seven more age-matched and gender-balanced case-control pairs in our study (Supplementary Fig. 1). These case-control pairs are 56-year-old female patients/58-year-old female control (pair 3); 61-year-old female patient/60-year-old healthy female (pair 4); 28-year-old female patient/44-year- old female healthy (pair 5); 33-year-old male patient/32-year-old female control (pair 6); and 68-year-old male patient/67-year-old male control (pair 7). All patients represent classic cases of ME/CFS with extreme muscle fatigue and severe cognitive impairment. Patient #3 and 4 further display orthostatic intolerance (OI), whereas patient #5 and 7 exhibited peripheral small fiber polyneuropathy along with OI, both frequent pathological findings in ME/CFS. The cohort was carefully structured to minimize variability in terms of geographical location, ethnicity, gender, age, disease onset, course of the disease, and timing of blood collection. Blood collection was performed with appropriate patient consent and based on the guidelines of an approved IRB protocol.

3.2. Estimation of protein aggregation propensities in serum samples of ME/CFS patients

Although autophagy is an intracellular mechanism and can be best studied in cellular assays, the unavailability of post-mortem ME/CFS tissue has limited such analyses. Nevertheless, severe impairment in autophagy might also result the increased tendency of protein aggregation in extracellular matrix such as serum and plasma (Giacomelli et al., 2017; Magalhães et al., 2020; Sharma, 2018). Aggregated proteins such as amyloid-β and α-syn are often detected in serum samples of AD and PD patients as a result of autophagy impairment. Thioflavin-T based fluorometric assay is one of the most reliable strategies to study protein aggregation. Although thioflavin-T based protein aggregation analysis has been utilized in cell-free systems, until now such a method strategy has not previously been brought to bear on serum samples. Here, we used a thioflavin T (ThT)-based biochemical assay to evaluate whether abnormal protein aggregation occurs in ME/CFS patient serum. The method is a fluorometric tracking analysis that generates a sigmoidal evolution of protein from its linear structure to aggregated morphology.

Serum samples of both a 74-year-old healthy control and a 71-year-old male ME/CFS (Fig. 1A) patient displayed increasing but non-linear pattern of aggregation as indicated with one-phase association non-liner fitted curve of florescence intensities (486 nm/450 nm) with the function of increasing time from 0 to 90 min of ThT addition. Interestingly, we observed that serum proteins of the patient displayed a significantly faster rate of protein aggregation compared to healthy control, as indicated with steeper slope of 70.70 ± 1.956 in patient compared to the relatively flat slope of 17.72 ± 0.3806 in the control. Moreover, the significance analysis revealed that there is a strong difference of protein aggregation rate in ME/CFS patient [$F_{29,29} = 15.99$ ($***p < 0.0001$)] compared to its sex-matched healthy control (Supplementary Table 1). Next, we performed a similar comparison study between 68-years-old healthy female and 67-year-old female ME/CFS patient (Fig. 1B), which resulted in a similar outcome of protein aggregation upon ThT addition. In that case-control pair, we also observed a significantly faster aggregation of serum proteins in the female patient compared to the healthy control (Supplementary Table 1) [$F_{29,29} = 15.99$ ($***p < 0.0001$)]. The non-linear fitted curve generated a steeper slope of 59.68 ± 3.005 in the patient vs. 19.36 ± 1.599 in the healthy control).

Furthermore. the data combined from $n = 7$ case-control pairs (Fig. 1C and Supplementary Table 1) indicated a strong tendency for protein aggregation in ME/CFS patients compared to age-matched healthy controls with a significantly high slope value (two-tailed paired *t*-test; $t = 8.445$, $df = 6$; $p < 0.0001$). Moreover, correlation analyses between the age of ME patients and the protein aggregation pattern did not display any strong relationship (Fig. 1D). Interestingly, combining slope values from $n = 8$ female and $n = 6$ male subjects in a scatter plot, we determined that 50% female and 20% male subjects display higher protein aggregation propensities as indicated with their distributions over median line (Fig. 1E). Taken together, these results indicate there is an increased protein aggregation pattern in the serum of ME/CFS patients compared to healthy controls.

3.3. Upregulation of autophagy markers in the serum of ME/CFS patients

Because increased protein aggregation might also indicate a defective autophagy proteome in serum (31856641), we performed a pilot study to evaluate the expression of autophagy markers in the serum samples of two ME/CFS patients. We carried out a human autophagy antibody array analysis (Supplementary Fig. 1C) in the serum of two case-control subjects. We observed that expression levels of ATG5, ATG7, ATG13, p62, Rheb, and α-syn were strongly upregulated in the serum sample of the 71-year-old ME/CFS patient (Fig. 2B; Supplementary Fig. 1B) compared to the age-matched healthy subject (Fig. 2A; Supplementary Fig. 1A). The result was further confirmed with a densitometric analyses (Fig. 2 Ci, Cii, Ciii, Civ, Cv, and Cvi are ATG 5, 7, 13, p62, Rheb, and α-syn respectively) with the significance of means calculated based on three independent experiments at $p < 0.0001$. To confirm the result, we performed ELISA analyses of ATG5, ATG13, p62 and α-syn in the serum sample of the male ME/CFS patient with commercially available kits. The detection sensitivity of these ELISA kits varies from lot to lot and is affected by the serum concentrations of proteins. Therefore, to demonstrate the accurate detection of these proteins, we adopted a dilution series of serum samples for ELISA-based detection of ATG5, ATG13, p62, and α-syn. A dose responsive non-linear fitting curve analysis followed by measuring the X intercept demonstrates that a 1:4 dilution of serum provides most efficient detection of these serum-derived factors (Supplementary Fig. 2A–C). Subsequent ELISA analyses revealed that ATG5 (Fig. 2D), ATG13 (Fig. 2E), p62

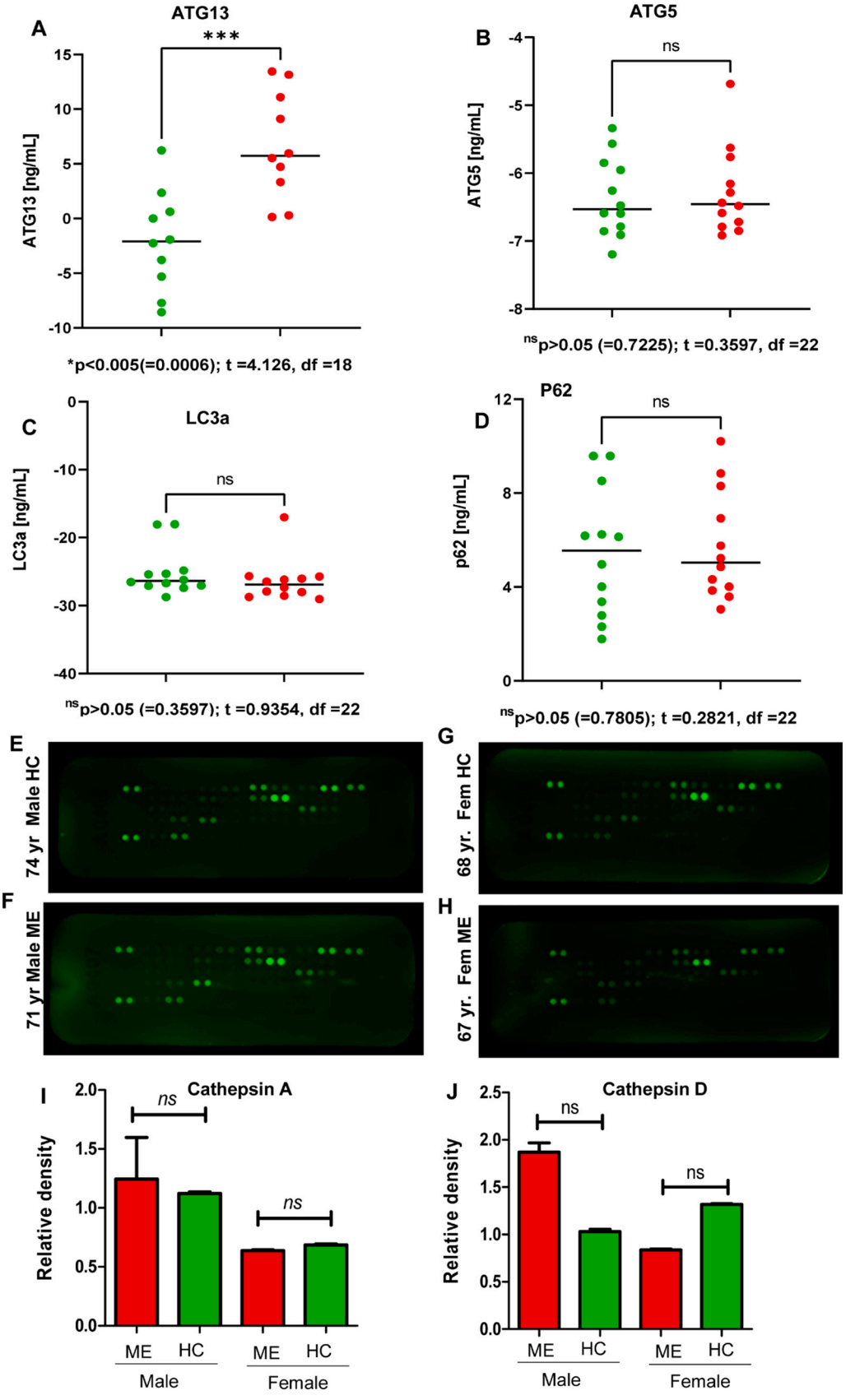

Fig. 3. Validating expression of autophagy markers in serum samples of $n = 11$ ME/CFS patients. A cohort of 11 healthy controls and 11 ME/CFS patients were analyzed for the expression of (A) ATG13, (B) ATG5, (C) LC3a, and (D) p62 in serum samples. Results are mean ± SD of three independent experiments. Significance of mean was tested with an unpaired t-test and resultant p values were presented underneath. Serum samples were diluted 1:5 (v/v) with assay diluent and then probed against 34 different proteases in a human protease profiler array (R& D systems; Cat # ARY021) membrane. Array analyses were performed in serum samples of (E) 74 years HC male, (F) 71 years male ME, (G) 68 years HC female, and (H) 67 years ME female. Relative densities of two important lysosomal enzymes (I) cathepsin A and (J) cathepsin D were calculated with respect to reference points and then plotted. Results were mean ± SD of three independent experiments. NS = not significant.

Table 1
Gender, ethnicity, age, disease status, and serum ATG13 (± SD) levels in a cohort of 24 subjects (12 healthy and 12 ME/CFS). High or low was determined with reference to mean (=4.8030). Expression above mean is considered to be high and below mean is considered to be low. Red = disease and Blue = control. OI = orthostatic intolerance; SFN = small fiber polyneuropathy; POTS = Postural Orthostatic Tachycardia Syndrome.

S/N	Status	Age	Gender	Ethnicity	Disease (Y/N)	ATG13 ng/mL	ATG13 (High/low)
1	Control	58	F	W	N	5.2438	high
2	Control	60	F	W	N	3.8755	low
3	Control	44	F	W	N	1.3909	low
4	CFS+, OI+, POTS+, SFN+	72	F	W	Y	11.299	high
5	SFN+ only, no CFS	83	M	W	Y	1.6975	low
6	Control	66	F	W	N	-4.298	low
7	CFS+, OI+, POTS+	40	F	W	Y	45.380	Very high
8	Control	25	M	W	N	3.933	low
9	CFS+, OI+, SFN+	66	F	W	Y	7.559	high
10	CFS+, OI+, SFN+	65	M	W	Y	4.999	high
11	Control	59	F	W	N	2.061	low
12	Control	59	F	W	N	22.547	high
13	Control	67	M	W	N	-7.765	low
14	Control	55	M	W	N	-2.682	Low
15	CFS+ only	73	M	W	Y	15.436	high
16	Control	68	F	W	N	-1.029	low
17	CFS+ only	33	M	W	Y	13.490	high
18	Control	32	M	W	N	-6.861	low
19	CFS+, OI+, SFN+	28	F	W	Y	7.8578	high
20	CFS+, OI+, SFN+	65	F	W	Y	16.087	high
21	Control	65	M	W	N	-0.6706	low
22	CFS+, OI+	56	F	W	Y	6.51124	high
23	CFS+, OI+	61	F	W	Y	-9.1545	low
24	CFS+ only	72	F	W	Y	7.377	high

(Fig. 2F), and α-syn (Fig. 2G) were strongly upregulated in serum samples of the 71-year-old ME/CFS patient, with the most significant elevation in ATG13 level, as evaluated with an unpaired *t*-test ($p < 0.0005 = 0.0003$ vs. healthy after 5 independent experiments). Although, ELISA is the most reliable technology to quantify serum proteins, sometimes a low signal-to-noise ratio in the HRP detection method limits the accurate quantification (Motsenbocker, 1988). Here we introduced a novel near infrared-based ELISA method, which produces extremely sensitive detection of low abundance proteins in serum mainly due to the high signal-to-noise ratio of the near-infrared probe (Jensen and Bak, 2002). Strong dark signals representing greater abundance of ATG5 (Fig. 2H), p62 (Fig. 2I), ATG13 (Fig. 2J), and α-syn (Fig. 2K) were observed in the serum sample of 71-year-old ME/CFS male compared to weak signals indicative of low levels of these proteins in the matched control. The specificity of the signal was validated by the absence of signal in a 2° antibody control, whereas equal loading was verified with total albumin. The result was further quantified with a densitometric analysis relative to total albumin concentration (Supplementary Fig. 3A). Collectively, these results indicate that the serum sample of the 71-year-old male ME/CFS patient displayed higher expression of ATG5, ATG13, p62, and α-syn, with the maximum difference in ATG13.

Next, we performed a similar antibody array analysis in the serum sample of the 67-year-old female patient, which indicated significant elevations of LC3a, LC3b, p62, α-syn, and ATG-13 proteins (Fig. 2M: Supplementary Fig. 1D) compared to the age-matched healthy control (Fig. 2L; Supplementary Fig. 1C). The result was further corroborated with densitometric analyses (Fig. 2Ni-2Nv). To nullify the possibility of unequal loading of protein in the array, we estimated the total protein concentration with the Bradford method (Bradford, 1976) before loading each sample on the array membrane. Since an antibody array is a semi-quantitative method to estimate serum protein, next we performed a quantitative ELISA analysis of LC3a, ATG5, ATG13, p62 and α-syn. Although, LC3a ELISA analyses (Fig. 2R) did not display significant differences, we observed strong elevations of ATG13 (Fig. 2O), p62 (Fig. 2P), and α-syn (Fig. 2Q) in the 67-year-old female ME/CFS patient compared to the healthy control with the maximum difference in ATG13 level ($p < 0.001$). Results were confirmed by five independent experiments.

Next, we performed a near-infrared ELISA assay for LC3a (Fig. 2S), ATG13 (Fig. 2T), p62 (Fig. 2U), and α-syn (Fig. 2V) with albumin as loading control. Similar to our quantitative ELISA method, no difference in LC3a expression was observed (Fig. 3L; Supplementary Fig. 3B). However, expression levels of ATG13, p62, and α-syn were consistently higher in the patient compared to the healthy control (Fig. 2T–V: Supplementary Fig. 3B). In both case-control experiments, we observed that serum levels of p62, α-syn and ATG13 were consistently elevated, suggesting that these patients might have significant impairment in the formation of autophagosomes. Based on these pilot data, we performed ELISA analyses of ATG13, ATG5, LC3a, and p62 in $n = 12$ healthy controls and n = 12 ME/CFS patients (Fig. 3A–D; Supplementary Fig. 4 for standard curves). Interestingly, we observed that only ATG13 (Fig. 3A), but not ATg5 (Fig. 3B), LC3a (Fig. 3C), and p62 (Fig. 3D) was found to be strongly elevated in the serum samples in $n = 10$ ME/CFS patients. The

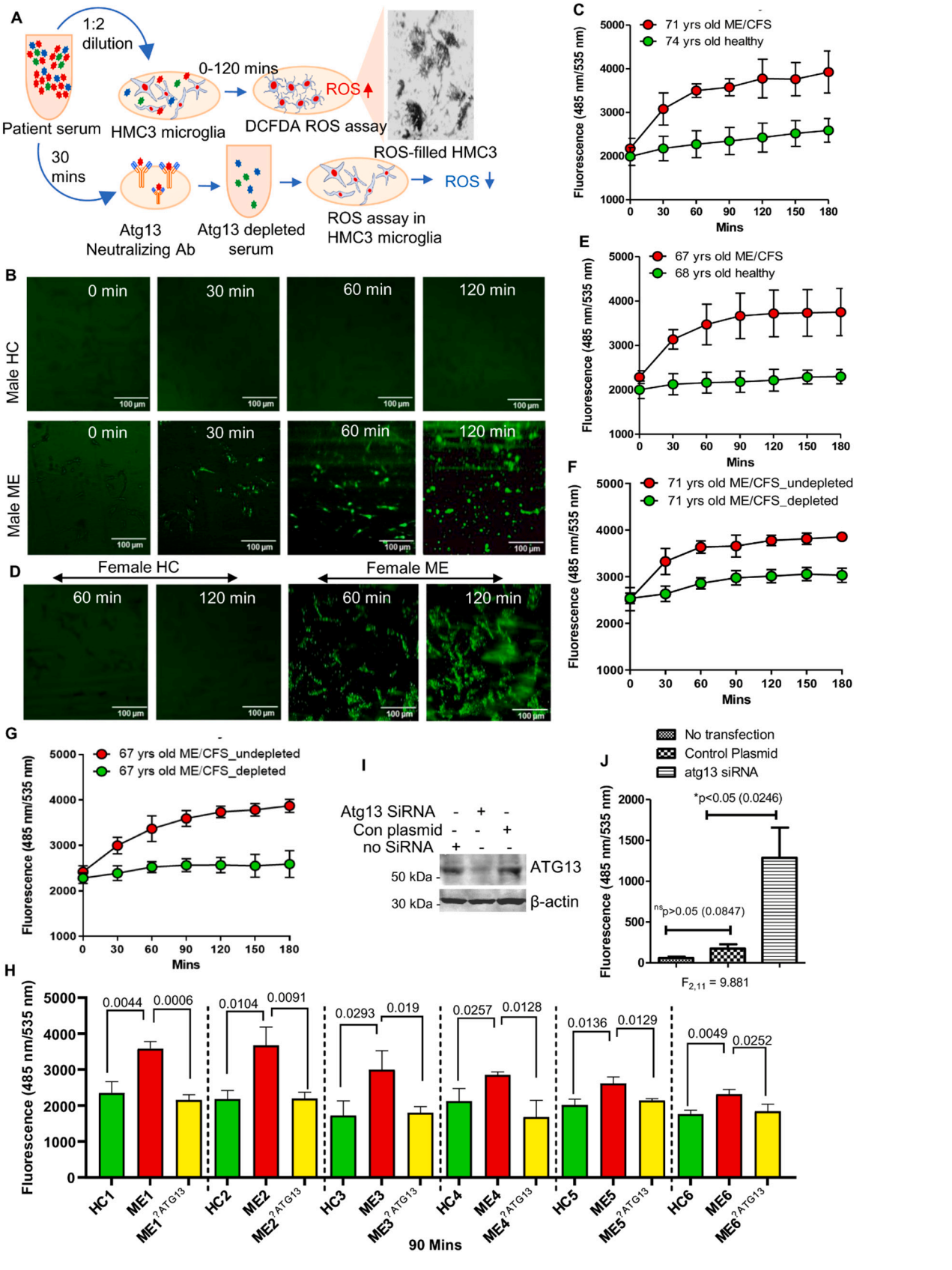

(caption on next page)

Fig. 4. Serum-derived ATG13 in ME/CFS patients evoked oxidative stress response in microglial cells. (A) A schema of the overall experimental plan. (B) HMC3 human microglial cells were treated with ME/CFS patient's serum (1:2 dil^{n}) supplemented DMEM media for 0 min, 30 mins, 60 mins, and 120 mins. The ROS production was assayed with DCFDA staining procedure. (C) Realtime ROS production was assayed in HMC3 microglia after stimulation with male healthy (green) and ME/CFS (red) subjects. A time-sensitive recording was performed at VictorX3 multichannel plate reader using 485 nm/535 nm wavelength (Ex/Em) protocol. A time-dependent ROS production assay was recorded at 485 nm/535 nm (Ex/Em) wavelength (D) HMC3 microglial cells were stimulated with sera (1:2 dil^{n}) of a female healthy and a ME/CFS patient for 60 and 120 mins followed by probing with DCFDA. Images were captured in FITC-filter of Hund fluorescence microscope. (E) Realtime ROS production was assayed at different time interval in HMC3 microglial cells once stimulated with sera of female healthy (green) and ME/CFS (red) subjects. (F) A similar ROS assay was performed in HMC3 cells after stimulation with the serum of a male ME/CFS patient (red) and ATG13-depleted serum (green). (G) A similar ROS assay was performed in presence of a female ME/CFS patient's serum and ATG13-depleted serum. (H) Fluorescence absorbance (485/535 nm) indicative of ROS production assay was done in HMC3 microglia after 90 min of incubation with $n = 6$ ME samples (red), HC controls (green), and ME samples neutralized with ATG13 (yellow). Unpaired *t*-test was done to compare significance between groups and displayed on the top. (I) IB of ATG13 and actin in microglial cells after *atg13* siRNA treatment. No treatment control and empty plasmid control were included. (J) ROS measurement was performed in *atg13*-siRNA treated microglial cells. Results were means ± SD of three independent experiments. (For interpretation of the references to color in this figure legend, the reader is referred to the web version of this article.)

detailed result is summarized in Table 1. Collectively, these data suggest that early autophagy marker ATG13 might be dysregulated in ME/CFS patients.

3.4. Evaluation of lysosomal function in ME/CFS patients

Upon enclosure in autophagosomes, cellular components are directed and fused to lysosomes for hydrolytic degradation (Lorincz and Juhasz, 2020). Therefore, we wanted to evaluate whether there is any lysosomal impairment in these patients. Lysosomes are the home of cathepsin, a class of acid proteases that play an essential role in the degradation of autophagic material and maintenance of the cellular homeostasis of metabolism (Repnik et al., 2012). Thus, lysosomal impairment can be evaluated by measuring the level of different cathepsins and other proteases. We adopted a human protease proteome profiler array, which can quantitatively detect 40 different blood-borne proteases (Supplementary Fig. 5) including cathepsins, kallikreins, and matrix metalloproteinases. Interestingly, we did not observe any difference in the expression of lysosomal cathepsins between the healthy control (Fig. 3E and the ME/CFS male patient (Fig. 3F), nor between the female control (Fig. 3G) and the male ME/CFS patient (Fig. 3H). Although strong signals were observed for lysosomal proteases such as Cathepsin A (Fig. 3I), D (Fig. 3J), and X (Supplementary Fig. 6A) in both case-control pairs, no significant differences were observed. We observed some upregulation of cathepsins in the male patient; however, that difference did not reach statistical significance. In contrast, we observed significant upregulation of extra-lysosomal proteases such as MMP-9 (Supplementary Fig. 6B) and proteinase-3 (Supplementary Fig. 6C) in the male but not the female ME/CFS patient.

3.5. Exploring the effect of autophagy marker ATG13 in the microglial stress response

Since we observed a strong upregulation of ATG13 in serum samples of ME/CFS patients, we wanted to study the functional significance of serum ATG13 in ME/CFS. Increased ROS production has been implicated in the pathogenesis of ME/CFS (Medow et al., 2013) and several other neuroinflammatory diseases such as Multiple Sclerosis (MS) (Roy et al., 2008), PD (Roy et al., 2012), and AD (Modi et al., 2015). A significant portion of these ROS, Reactive Nitrogen Species (RNS), and other inflammatory molecules is produced due to severe activation of microglia, CNS -resident inflammatory cells. Therefore, we wanted to study whether serum-derived ATG13 stimulated the production of ROS in microglial cells. In order to explore the effect of ATG13 on microglial ROS production, we created an in vitro cell culture model (Fig. 4A) in which HMC3 human microglial cells were treated with patient serum-constituted DMEM media (1:1 v/v) followed by measurement of ROS load in different time periods starting from 30 mins to 2 h. with the DCFDA staining procedure (Roy et al., 2008). As a control, healthy serum-constituted media was added on HMC3 cells and evaluated for ROS production. Our immunofluorescence analyses (Fig. 4B) revealed that serum from an ME/CFS patient but not control serum time-dependently increased the ROS production. The DCFDA-labelled ROS signal appeared as early as 30 min and reached maximum at 120 min. This semi-quantitative analysis was further confirmed with a real-time kinetic study (Fig. 4C), in which ROS production was measured at a ratio of 485/535 nm as a function of increasing time. We observed that serum sample of a male patient increased microglial ROS production with increasing time, whereas healthy serum did not evoke any ROS production. Next, we performed similar fluorescence imaging (Fig. 4D) and kinetic (Fig. 4E) analyses with serum samples of a female ME/CFS patient and age-matched healthy control. We observed that the patient serum elevated ROS production with increasing time. Taken together, these results established a new cell culture model to evaluate the ROS-inducing capacity in serum samples of ME/CFS patients. With the aid of this model, we were able to quantify ROS-production in HMC3 human microglial cells upon stimulation with ME/CFS serum.

Next, we wanted to examine the role of ATG13 in ME/CFS serum in augmenting ROS production in HMC3 microglial cells. We adopted a neutralization technique (Fig. 4A; lower panel), in which patient sera were added to a 96 well plate that is pre-coated with ATG13 neutralization antibody. After 30 min, ATG13-depleted sera (ME$^{\Delta ATG13}$) were carefully harvested from the top. These sera were then used in similar set of experiments to evaluate microglial ROS production. ATG13-depleted sera of both male (Fig. 4F) and female patients (Fig. 4G) caused significantly lower production of ROS in HMC3 cells than ATG13-replete sera, suggesting a direct role of serum-derived ATG13 in stimulating oxidative stress in microglial cells. Data from $n = 6$ other cases of ME/CFS patients (Fig. 4H) provided consistent results, suggesting that ME/CFS serum-derived ATG13 directly induces ROS production in cultured HMC3 microglial cells.

However, it is not known whether ATG13-mediated ROS production is purely an extracellular event or whether intracellular ATG13 also participates in ROS production. Interestingly, an *atg13* siRNA (Cat # 122699; human; ThermoFisher) that mediates knock -down of *atg13* gene expression (Fig. 4I) evoked significant ROS production in microglial cells (Fig. 4J), suggesting that the intracellular ATG13 actually mitigates microglial ROS production. Similar siRNA knock-down of other autophagy -related proteins such as ATG5 (PMID: 34336554) and Beclin (24452380) also induced ROS productions in microglia.

Next, we wanted to study if ATG13 could directly stimulate NO production in microglia. Total NO (sum of nitrite and nitrate) in microglial supernatant was measured via a fluorimetric-based assay procedure as described in method section. Surprisingly, 1:8, 1:4 (25, and 1:2 (12.5, 25, and 50 μL serum in 87.5,75, and 50 μL serum-free DMEM/F12 media respectively) dilutions (v/v) of serum from the male ME/CFS patient, dose-dependently stimulated NO production in HMC3 microglial cells (Fig. 5A; red bars; Supplementary Fig. 7A & B for standard curve). Accordingly, NO production was found to be significantly higher in the supernatants of $n = 8$ ME/CFS serum-treated HMC3 microglial cells measured after 24 h. Interestingly, ME$^{\Delta ATG13}$ serum samples were unable to evoke NO production in microglial cells (Fig. 5B) suggesting

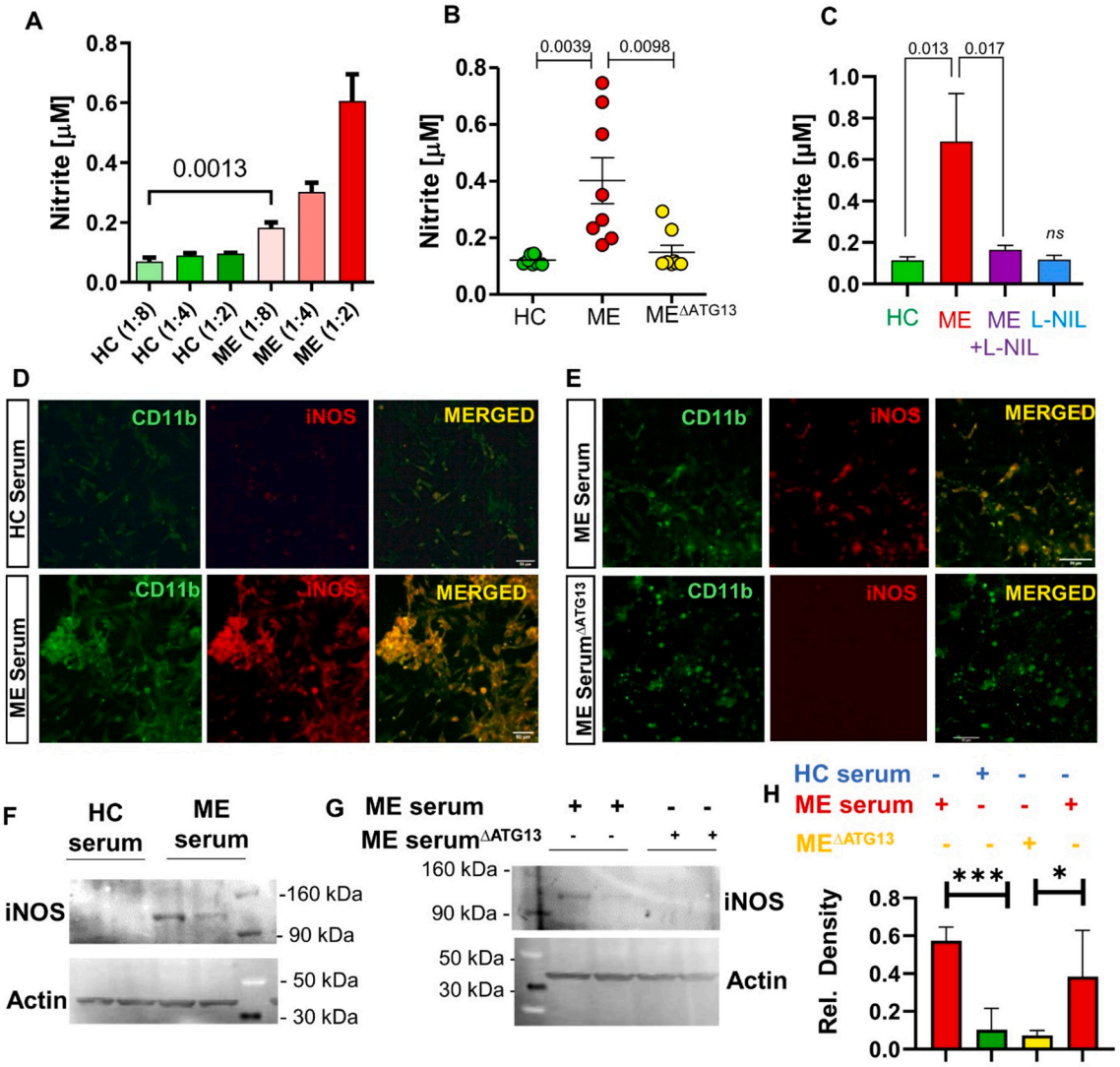

Fig. 5. Effect of serum-derived ATG13 on the production of nitric oxide (NO) in HMC3 microglial cells. (A) HMC3 microglial cells were stimulated with increasing doses of HC serum (green; 74-year–old male HC) and ME serum (red; 71-year-old male ME). Before applying on microglia, serum samples were diluted at 1:2,1:4, and 1:8 dilution (diluted with serum-free DMEM media) for 24 h. After 24 h, nitric oxide production was measured by thefluoremetric detection method. Two-way ANOVA was performed to measure the significance between groups considering dose and disease status as two independent factors. While analyzing the effect of dose on the significance between groups, the descriptive statistics is $F_{2,9} = 6.368284$ ($>F_c = 3.55$): $p < 0.001$ (=0.00814). On the other hand, when comparing between HC and MS, the significance test resulted $F_{2,9} = 3.224176$ ($>F_c = 2.45$): $p < 0.05$(=0.016). (B) NO production was confirmed in serum samples of $n = 8$ ME patients. The significance of mean was tested with one-way ANOVA. Descriptive statistics fo the significance between group is $F_{2,21} = 9.925$: $p < 0.01$(=0.0009). Green dots for HC, red dots for ME, and yellow dots for ATG13-depleted ME serum samples. (C) L-NIL (25 μM) was treated on microglia for 2 h followed by the treatment with ME serum (1:2 dil) and after another 22 h, NO production was measured in HMC3 microglia. One-way ANOVA to test the significance between groups resulted $F_{3,8} = 17.02$: $p < 0.01$(=0.0008). (D) Dual immunofluorescence (IF) analyses of CD11b (green) and iNOS (red) in HMC3 microglia treated with HC and ME serum (1:2 dilution) for 24 h. (E) Dual IF analyses for CD11b and iNOS in microglia treated with ME serum and ME serum (1:4 dilution) neutralized with ATG13 antibody. IB analyses of iNOS and actin in microglia treated with (F) ME and HC serum (1:2 dilution) and (G) ME serum and ATG13-neutralized ME serum (1:2 dilution). (H) Densitometric analyses was done after normalizing with respective actin bands. Results are mean ± SD of three independent experiments. The significance of mean was tested with unpaired t-test with $*p < 0.05$ and $***p < 0.0001$. (For interpretation of the references to color in this figure legend, the reader is referred to the web version of this article.)

that serum-derived ATG13 plays a direct role in the microglial production of NO. Upregulation of NO could be due to the direct stimulation of iNOS enzyme in HMC3 microglial cells. To evaluate that, Microglial cells were stimulated with 25 μM of L-NIL, a pharmacological inhibitor of iNOS, followed by the stimulation with 1:2 dilution of ME serum. Interestingly, ME serum was found to be ineffective towards NO production once iNOS is inactivated (Fig. 5C; Supplementary Fig. 7C) in microglia. One potential confounder of this study is the endogenous NO in ME serum samples that could interfere with the conclusion. To nullify that, we measured NO in both HC and ME serum samples ($n = 7$ per group; Supplementary Fig. 7D) indicating that there was no difference in NO levels between HC and ME serum samples. Immunocytochemical analyses of CD11b (microglial marker) and iNOS clearly demonstrated that there was a strong upregulation of iNOS in microglial cells treated with ME serum (Fig. 5D), but not with $ME^{\Delta ATG13}$ serum (Fig. 5E), further indicating that ME serum-derived ATG13 strongly upregulated the cellular expression of iNOS in human microglial cells. The upregulation of iNOS in microglia by ME/CFS serum was further corroborated with immunoblot (IB) analyses (Fig. 5F), whereas reduction of iNOS in microglia by $ME^{\Delta ATG13}$ was also confirmed with an IB analysis (Fig. 5G), followed by densitometric evaluations (Fig. 5H). Taken together, these results suggest that elevated ATG13 in the serum of ME/CFS patients

directly stimulates oxidative stress and iNOS-induced NO production in microglial cells.

3.6. Serum-derived ATG13 employs microglial surface receptor RAGE to evoke ROS and Nitric oxide

Microglia express a huge repertoire of surface receptors including pattern recognition receptors, integrins, purinergic receptors, aryl hydrocarbon receptors, cytokine receptors, and ion channels. These

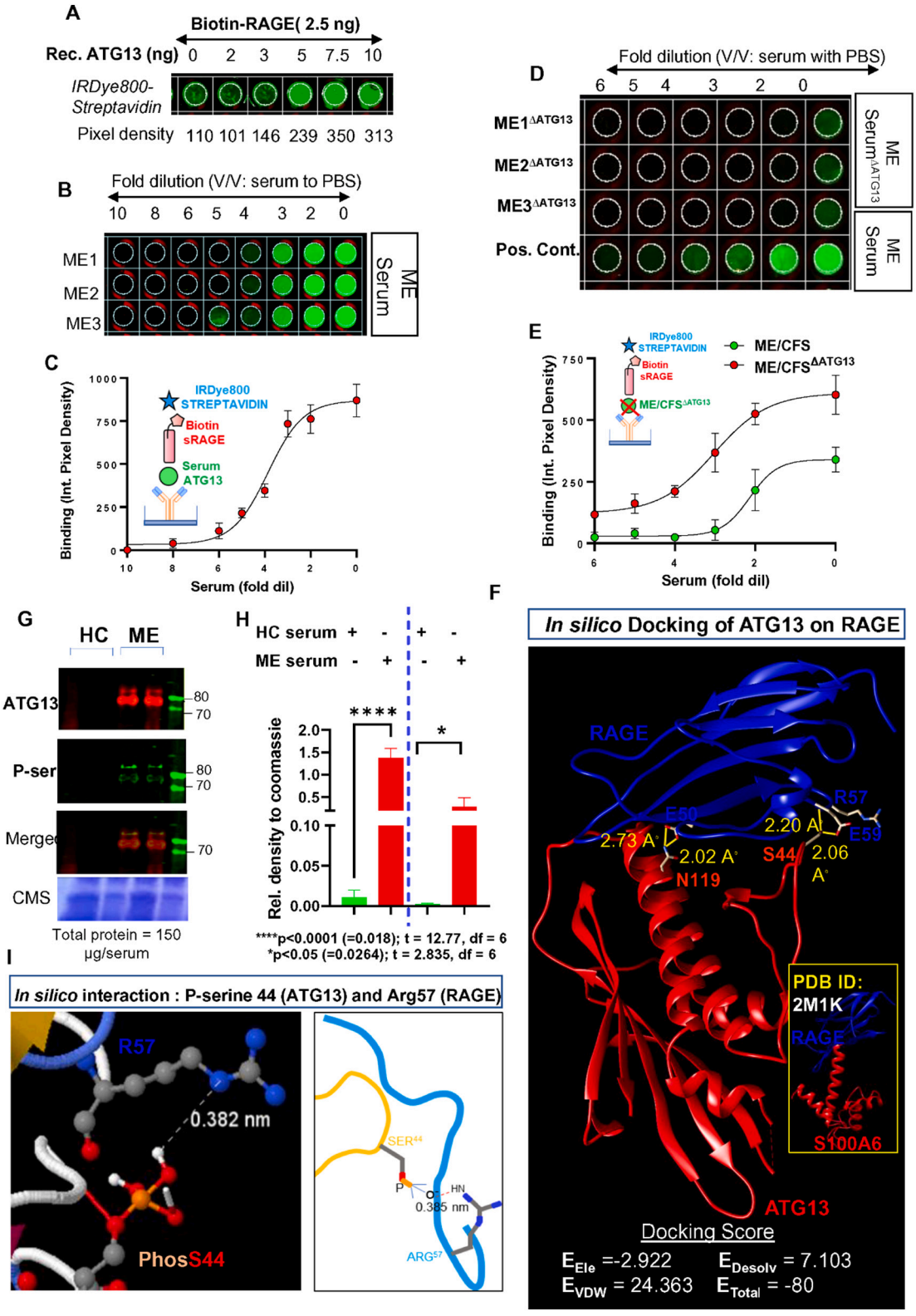

(caption on next page)

Fig. 6. Serum-derived ATG13 binds with surface receptor RAGE in microglia. (A) Increasing concentrations of recombinant ATG13 (0, 2, 3, 5, 7.5, and 10 ng/mL) were coated in a 96 well plate following incubation with biotinylated extracellular domain of human RAGE receptor and then detection with IRdye800-tagged streptavidin in Li-Cor Odyssey Sa 96-well plate reader. Resultant integrated densities (average of three readings) were pasted underneath. (B) ME/CFS serums from 3 randomly selected cases were serially diluted from 2- to 10-fold and then applied to an ATG13 antibody coated plate and then probed with biotinylated RAGE receptor. (C) The binding was plotted with non-liner regression curve showing a sigmoidal binding curve. Results were mean ± SD of three samples. Similar binding analyses with three ATG13-neutalized ME serum samples were displayed in a plate format (D) and with a non-liner sigmoidal binding curve (E). (F) In silico docking analyses of ATG13 (red) in the extracellular surface of RAGE. Homology modeling was performed in SwissDock server considering RAGE and S100A6 crystal structure (PDB ID: 2M1K) as a template. The most stable configuration was displayed with strongest docking score given underneath. (G) Freshly harvested serum samples of HC and ME/CFS cases were purified through protein A agarose to remove IgG followed by immunoblot analyses of total ATG13 (1:100) and phospho-serine (1:100) antibodies. Total protein was estimated with Coomassie (CMS) blue staining of these samples. (H) Relative density of ATG13 and phospho-serine to Coomassie was plotted. ATG13 and phospho-serine plots were divided with dotted line. (I) Based on in-silico analysis, A conserved serine residue at Ser 44 surrounded by Ser 42 and Ser43 is likely to be phosphorylated. The structure indicates that phosphorylated Ser44 might engage in a H-bond interaction with the critical Arg 57 of RAGE. (For interpretation of the references to color in this figure legend, the reader is referred to the web version of this article.)

receptors engage in direct interactions with almost all extracellular neurotoxic stimuli and Blood Brain Barrier (BBB) -infiltrated peripheral immune cells and can cause severe inflammation in the central nervous system. Therefore, we wanted to identify the receptor for serum-derived ATG13. Activation of RAGE has been shown to directly induce ROS and NO productions in microglial cells. We first adopted a dose-responsive receptor-ligand assay in which increasing doses of recombinant ATG13 protein (Abcam; Cat #ab127606) were challenged with 2.5 ng of biotinylated-RAGE (Aviscera Bioscience; Cat # 00112–02-50B) followed by IRDye800-strepatvidin (Li-cor Bioscience) treatment for IR-based signal detection. The increasing concentrations of ATG13 demonstrated dose-dependent binding with RAGE (Fig. 6A), generating a sigmoidal binding curve with EC50 = 4.5 and Hill slope = 5.116 (Supplementary Fig. 8A). Surprisingly, three different ME/CFS patient serums displayed a strong binding affinity towards biotinylated-RAGE protein. ME/CFS serums were serially diluted up to 10-fold (Fig. 6B) and added onto ATG13 antibody-coated plates. Strong binding was observed at 0- to 2- fold dilution (Fig. 6C). However, the binding is markedly inhibited with $ME^{\Delta ATG13}$ serum samples ($n = 3$) (Fig. 6D & E). An in-silico homology modeling study (Template: 2M1K between RAGE and S1006A; inset) revealed that there could be a strong interaction of ATG13 with the extracellular ligand binding domain of RAGE (Fig. 6F). Literature (Xie et al., 2008) suggests that Glu 59 and Arg 57 of RAGE are two critical residues that regulate structural changes in RAGE during its binding with ligands. In particular, Arg 57 mediates water molecule-based passive H-bonding with ligands such as protein S100B (Jensen et al., 2015). Interestingly, our docking analysis revealed that Ser44 residue of ATG13 could engage multiple H-bond interactions with Glu59 (Fig. 6F). While examining the neighboring amino acid residues of Ser44 in ATG13 (NCBI Ref. Seq # NP_001192048.1), we found that there are four consecutive serine residues, including Ser41, Ser42, Ser43, and Ser44.

ATG13 is heavily phosphorylated by intracellular kinases such as AMPK and mTOR. An immunoblot analysis of ATG13 in protein A-agarose purified and freshly preserved serum (2 ME/CFS and 2 HC) clearly indicated that there was a strong upregulation of ATG13 and that the signal resolved into two bands of different molecular mass. (Fig. 6G and H). Further probing with pan phosphoserine antibody clearly identified the higher band as a phosphor-ATG13 (Fig. 6G) indicating that some of the ATG13 in ME/CFS serum is phosphorylated. A subsequent in silico study indicated that phosphorylation of ATG13 at Ser44 could make a potential H-bond interaction with Arg57 residue of RAGE (Fig. 6I).

Next, we wanted to investigate whether neutralization of RAGE could prevent the oxidative stress-inducing activity of ME serum samples in microglia. RAGE neutralizing antibody (R&D Systems; Cat # AF1145) was first evaluated for its ability to nullify the interaction between ATG13 and RAGE (Fig. 7A). Our results indicated a significant inhibition of binding at 7–10 μg/mL (>0.35 μg/50 μL based on assay) of RAGE-neutralizing antibody (Fig. 7B). Blocking RAGE in microglia ($HMC3^{\Delta RAGE}$) significantly attenuated the ME/CFS serum-induced ROS production (Fig. 7C), which we confirmed in a time-sensitive study (Fig. 7D). Accordingly, ME/CFS serum was found to be ineffective to induce iNOS expression in $HMC3^{\Delta RAGE}$ microglial cells (Fig. 7E), a finding that we confirmed with an iNOS immunoblot (Fig. 7F). Taken together, our results indicate that serum samples of ME/CFS patients have elevated ATG13 proteins indicative of a biochemical impairment of autophagy. Our data further demonstrate that the serum-derived ATG13 is phosphorylated and employs the RAGE receptor to induce oxidative stress response in microglial cells.

4. Discussion

ME/CFS is a debilitating chronic disorder characterized by diverse pathological symptoms including muscle pain, fatigue, post-exertional malaise, dizziness, cognitive impairment, and chronic inflammation. Although, the, molecular mechanism of this disease is still obscure, recent literatures suggest that the impairment in mitochondrial function is critical in the development of immune dysregulation, fatigue, and cognitive deficit in ME/CFS patients. Autophagy is a quality control process that regulates mitochondrial homeostasis in healthy cells. However, it is not known if autophagy is impaired in ME/CFS pathogenesis. Several lines in this report provide evidence for an impaired autophagy function in ME/CFS patients. First, a ThT-based protein aggregation study revealed that serum samples of ME/CFS patients had significantly higher propensity to form aberrant protein aggregates which should have been removed by the autophagy system by the degradation in lysosomes. Second, our dot blot antibody array analyses indicated that serum levels of autophagic proteins such as ATG5, ATG7, ATG13, p62, and α-syn were strongly elevated in a 71-year-old male ME/CFS patient. A similar antibody array analysis in a 67-year-old female patient detected significantly high levels of ATG13, LC3a, LC3b, p62, and αsyn. Third, competitive ELISA analysis displayed that early autophagy protein ATG13 was strongly elevated in the serum of 10 ME/CFS patients compared to age-matched healthy controls. Fourth, our near-infrared ELISA analyses confirmed strong upregulation of ATG13, p62, and α-syn in serum of these patients. All these results imply that there could be a substantial impairment of autophagy in ME/CFS patients.

To evaluate aberrant protein aggregation in serum we applied ThT-based protein aggregation strategy in serum samples. A kinetic study was previously performed to observe amyloid-β protein aggregation (Meng et al., 2008) in a cell-free system (Batzli and Love, 2015). In our present study, we adopted similar fluorimetric tracking methods to explore whether the serum proteins of ME/CFS patients have higher propensities to form aggregates. The accelerated rate of aggregation we detected does not necessarily reflect an impairment of the physiological mechanism of protein degradation; however, it might indicate that there is a higher tendency to form aberrant protein aggregates in serum samples of ME/CFS patients.

Although the detection of ATG13 in blood serum was unexpected, our results have demonstrated that serum samples of ME/CFS patients ($n = 10$) have significantly high level of ATG13 compared to age-matched and gender-balanced healthy controls. Competitive ELISA

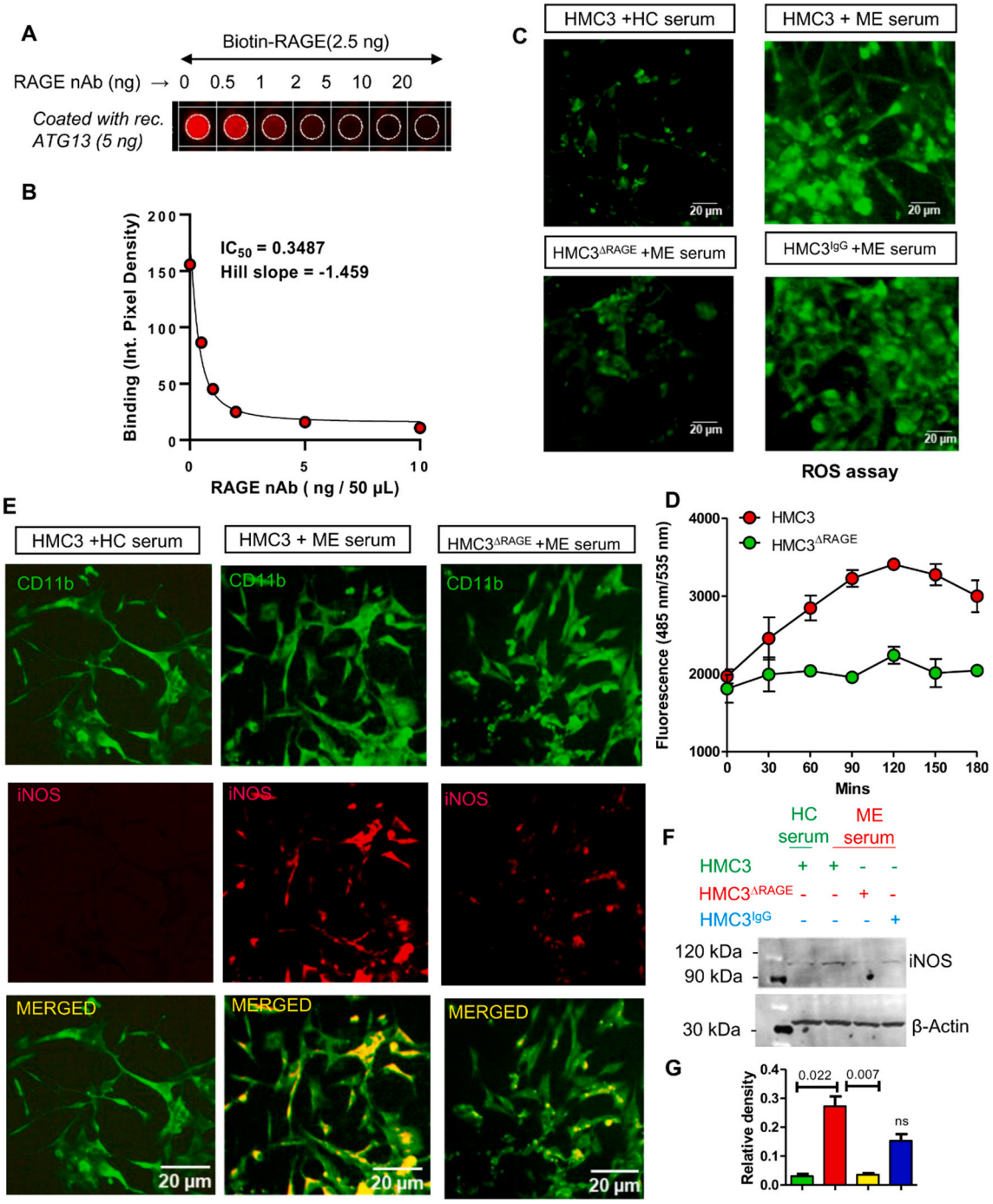

Fig. 7. Functional blocking of RAGE receptor nullifies ME serum to induce ROS and iNOS expression in HMC3 human microglia. (A) Serially diluted RAGE neutralizing antibody (Cat # AF1145: R&D systems) incubated with biotinylated RAGE and then added to 96 well plate precoated with recombinant-ATG13 (5 ng/well) protein. The binding between ATG13 and RAGE was visualized with IRDye800-tagged streptavidin dye. (B) A sigmoidal inhibition plot of RAGE-ATG13 binding (Y axis) with increasing RAGE blocking antibody (X axis) that displays $IC_{50} = 0.3487$ (equivalent to 7 µg/mL) and hill slope = −1.459. Non-liner regression curve was plotted in GraphPad Prism 9 software. HMC3 microglial cells are neutralized with 10 µg/mL RAGE antibody or IgG for 30 mins), washed with 1× PBS, inserted with DCFDA dye for1 hr, and then treated with HC serum or ME serum for 0, 30, 60, 90, and 120 mins. (C) Representative images were taken after 90 min of incubation. (D) A realtime ROS assay plot with DCFDA fluorescence evoked as a function of time plotted. Results are mean ± SD of 3 different experiments. (E) immunocytochemical analyses of CD11b (green) and iNOS (red) in HMC3 microglial cells treated with HC serum (first column), ME serum (2nd column), and in RAGE neutralized (10 ng/mL) HMC3 microglial cells treated with ME serum (third column). Treatment was done for 24 h with serum. (F) IB analyses followed by (G) densitometry of iNOS once normalized with beta-actin in RAGE-neutralized microglia after similar treatment condition. Results are mean ± SD of three independent experiments. (For interpretation of the references to color in this figure legend, the reader is referred to the web version of this article.)

analyses, near-infrared ELISA, antibody array, and IB analyses collectively confirmed that there was a strong upregulation of ATG13 in ME/CFS serum. A recent report suggests that an increase in the level of ATG proteins in serum, specifically ATG5 and ATG12, might lead to progressive neuronal damage in brain of AD patients (Cho et al., 2019). Aberrant aggregation of amyloid-β in the AD brain stimulates the impairment of autophagy, resulting the release of ATG5 and ATG12 into cerebrospinal fluid (CSF) and blood serum. Release of phospho-ATG13

in blood might be related to the cognitive impairment experienced by ME/CFS patient. In fact, the 71-year-old ME/CFS patient in our study, who displayed very high level of phospho-ATG13 in his serum, also exhibits significant cognitive impairment and memory loss. Additionally, we observed a strong upregulation of α-syn in his serum indicating a potential correlation of ATG13 with α-syn in Lewy body disease (Roy and Pahan, 2013; Roy et al., 2016) with ME/CFS. Lewybody dementia is often accompanied with severe microglial activation (Streit and Xue, 2016; Surendranathan et al., 2018). In fact, we observed that serum-derived ATG13 significantly stimulated oxidative and nitrosylative stress response in microglial cells. Our study indicates that ME serum promotes the expression of iNOS-derived NO in microglia, which has neurodegenerative and inflammatory implications in the pathogenesis of ME/CFS. However, NO is a double-edged sword (Mocellin et al., 2007; Yuste et al., 2015) as its productions from constitutive NOS such as neuronal NOS (nNOS) (Bonthius et al., 2008) and endothelial NOS (eNOS) (Osuka et al., 2008) have been reported to be beneficial. NNOS -derived NO displays neuroprotective functions, whereas eNOS-derived NO ameliorates diabetic cardiomyopathy (Sun et al., 2020). Interestingly, a recent study (Bertinat et al., 2022) indicates that ME/CFS plasma inhibits NO production via inactivation of endothelial NOS in cultured human umbilical vein endothelial cells directly contributing to the endothelial dysfunction (ED) in subset of ME patients. Therefore, based on its enzymic production, NO could be a double-edged sword in the pathogenesis of ME/CFS. Interestingly, Selective neutralization of ATG13 in ME/CFS serum significantly attenuated microglial production of NO and ROS. Interestingly, attenuation of intracellular ATG13 displayed an opposite effect by stimulating the production of ROS indicating that extracellular, but not intracellular ATG13, is metabolically toxic.

Apart from these neurotoxic implications, serum ATG13 is also correlated with cardiomyopathy. A recent study (Zhao et al., 2021) indicates that during myocardial infarction, the plasma level of ATG13 rises and that selective inhibition of circulating ATG13 is protective against myocardial infarction and other cardiovascular impairments. Interestingly, we observed that a 67-year-old female patient in our present study with significantly high level of serum ATg13 also suffers from cardiovascular abnormalities with exceptionally high blood pressure, which could be related to the high level of circulating ATG13. ATG13 also regulates the expression of antiviral interferon β to restrict viral infection and plays an essential role in innate immune response to provide antiviral immunity (Du et al., 2019). ATG13 participates in the early stage of autophagy vesicle formation process via forming a complex of *ULK1* (unc-51 like autophagy activating kinase 1), FIP200 (Hara et al., 2008), and ATG101 (Zachari and Ganley, 2017). Activation of mammalian target of rapamycin (mTOR) directly causes hyperphosphorylation of ATG13 in multiple serine residues (Puente et al., 2016), inhibits the formation of ULK1 complex, and subsequently aborts the autophagy process resulting the accumulation of aberrant proteins and depolarized mitochondria in the biologically active cell. While characterizing the biochemical properties of serum-derived ATG13, we also observed that ATG13 is phosphorylated at its serine residue.

Our In-silico analysis followed by functional binding assay suggest that ATG13 interacts with RAGE receptor in microglial cells to induce ROS and NO productions. Activation of RAGE and subsequent production of ROS and NO have been frequently reported in alpha-synucleinopathy (Haines et al., 2018; Jiang et al., 2018) and amyloid β-induced (Donahue et al., 2006) neurotoxicity. Interestingly, our in-silico study has predicted that a serine-rich N-terminal domain of ATG13 directly binds to the extracellular domain of RAGE and that binding is reinforced once Ser44 of ATG13 is phosphorylated. Interestingly, a recent report suggests that upon phosphorylation, ATG13 aborts the autophagy process (Chan, 2009; Hosokawa et al., 2009)and gets released to serum, suggesting that phosphorylated ATG13 in ME/CFS patients might contribute to the impairment of the cellular autophagy process.

ME/CFS patients are highly heterogeneous in terms of pathophysiological outcomes and serum marker proteins. The cohort we analyzed is age-matched, gender-balanced, and geographically confined, thus offering a significant homogeneity. However, as a future direction, we need to analyze the finding in larger cohort of $n = 100$ samples from geographically diversified populations. The upstream regulator of ATG13 phosphorylation needs to be characterized. Taken together, our experiments provide molecular evidence of autophagy impairment in ME/CFS.

Data availability statement

There is no electronic datasheet associated with this paper. Raw blots, standard curve of ELISA, and layout of the array were included in the supplemental file. Data associated with patients' clinical history has been preserved and restricted by Western IRB to DP. No data in electronic repository.

Ethical statement

Acquisition of patients' serum, documentation of questionnaire, collection of written consent, and other procedures in this study were conducted in accordance with the Sierra internal medicine-approved western IRB # 20201812 protocol.

Contributions of authors

GC, RW, MM, KK, and AR conducted experiments; DP obtained IRB approval, diagnosed subjects, and maintained a biobank; AR conceived the idea, designed experiments, and wrote the manuscript.

Declaration of competing interest

Authors declare no conflict of interest.

Acknowledgement

This work was supported by Simmaron Research Inc., a non-profit 501C research organization, Incline Village, NV 89451, as a result of funds from generous private donors. We thank the human subjects for their participation. We thank Dr. Maureen Hanson for manuscript editing and helpful suggestions.

Appendix A. Supplementary data

Supplementary data to this article can be found online at https://doi.org/10.1016/j.mcn.2022.103731.

References

Ahmed, I., Liang, Y., Schools, S., Dawson, V.L., Dawson, T.M., Savitt, J.M., 2012. Development and characterization of a new Parkinson's disease model resulting from impaired autophagy. J. Neurosci. 32, 16503–16509.

Anon, 2015. Beyond myalgic encephalomyelitis/chronic fatigue syndrome: redefining an illness, 180, 721–723.

Armstrong, C.W., McGregor, N.R., Lewis, D.P., Butt, H.L., Gooley, P.R., 2015. Metabolic profiling reveals anomalous energy metabolism and oxidative stress pathways in chronic fatigue syndrome patients. Metabolomics 11, 1626–1639.

Batzli, K.M., Love, B.J., 2015. Agitation of amyloid proteins to speed aggregation measured by ThT fluorescence: a call for standardization. Mater. Sci. Eng. C Mater. Biol. Appl. 48, 359–364.

Benes, P., Vetvicka, V., Fusek, M., 2008. Cathepsin D—many functions of one aspartic protease. Crit. Rev. Oncol. Hematol. 68, 12–28.

Bertinat, R., Villalobos-Labra, R., Hofmann, L., Blauensteiner, J., Sepúlveda, N., Westermeier, F., 2022. Decreased NO production in endothelial cells exposed to plasma from ME/CFS patients. Vasc. Pharmacol. 143, 106953.

Bonthius, D.J., Bonthius, N.E., Li, S., Karacay, B., 2008. The protective effect of neuronal nitric oxide synthase (nNOS) against alcohol toxicity depends upon the NO-cGMP-PKG pathway and NF-kappaB. Neurotoxicology 29, 1080–1091.

Bougea, A., Stefanis, L., Paraskevas, G.P., Emmanouilidou, E., Vekrelis, K., Kapaki, E., 2019. Plasma alpha-synuclein levels in patients with Parkinson's disease: a systematic review and meta-analysis. Neurol. Sci. 40, 929–938.
Bradford, M.M., 1976. A rapid and sensitive method for the quantitation of microgram quantities of protein utilizing the principle of protein-dye binding. Anal. Biochem. 72, 248–254.
Buchwald, D., Cheney, P.R., Peterson, D.L., Henry, B., Wormsley, S.B., Geiger, A., Ablashi, D.V., Salahuddin, S.Z., Saxinger, C., Biddle, R., 1992. A chronic illness characterized by fatigue, neurologic and immunologic disorders, and active human herpesvirus type 6 infection. Ann. Intern. Med. 116, 103–113.
Castellazzi, M., Patergnani, S., Donadio, M., Giorgi, C., Bonora, M., Bosi, C., Brombo, G., Pugliatti, M., Seripa, D., Zuliani, G., Pinton, P., 2019. Autophagy and mitophagy biomarkers are reduced in sera of patients with Alzheimer's disease and mild cognitive impairment. Sci. Rep. 9, 20009.
Cerri, S., Blandini, F., 2019. Role of autophagy in Parkinson's disease. Curr. Med. Chem. 26, 3702–3718.
Chan, E.Y., 2009. mTORC1 phosphorylates the ULK1-mAtg13-FIP200 autophagy regulatory complex. Sci Signal 2, pe51.
Cho, S.-J., Lim, H.J., Jo, C., Park, M.H., Han, C., Koh, Y.H., 2019a. Plasma ATG5 is increased in Alzheimer's disease. Sci. Rep. 9, 4741.
Demircan, G., Kaplan, O., Ozdas, S.B., 2018. Role of autophagy in the progress of coronary total occlusion. Bratisl. Lek. Listy 119, 103.
Donahue, J.E., Flaherty, S.L., Johanson, C.E., Duncan 3rd, J.A., Silverberg, G.D., Miller, M.C., Tavares, R., Yang, W., Wu, Q., Sabo, E., Hovanesian, V., Stopa, E.G., 2006. RAGE, LRP-1, and amyloid-beta protein in Alzheimer's disease. Acta Neuropathol. 112, 405–415.
Du, J.L., Ma, P., Wang, C., Zeng, Y., Xue, Y.J., Yang, X.C., Wan, X.M., Chang, F.F., Zhao, T.Y., Jia, X.Y., Wang, H.Z., Liu, J., Ma, Z.R., Cao, X., Cai, K.Z., 2019. ATG13 restricts viral replication by induction of type I interferon. J. Cell. Mol. Med. 23, 6508–6511.
Eskelinen, E.-L., 2006. Roles of LAMP-1 and LAMP-2 in lysosome biogenesis and autophagy. Mol. Asp. Med. 27, 495–502.
Evans, C.S., Holzbaur, E.L.F., 2020. Lysosomal degradation of depolarized mitochondria is rate-limiting in OPTN-dependent neuronal mitophagy. Autophagy 16, 962–964.
Filler, K., Lyon, D., Bennett, J., McCain, N., Elswick, R., Lukkahatai, N., Saligan, L.N., 2014. Association of mitochondrial dysfunction and fatigue: a review of the literature. BBA Clinical 1, 12–23.
Giacomelli, C., Daniele, S., Martini, C., 2017. Potential biomarkers and novel pharmacological targets in protein aggregation-related neurodegenerative diseases. Biochem. Pharmacol. 131, 1–15.
Haines, D.D., Trushin, M.V., Rose, S., Bernard, I.A.S., Mahmoud, F.F., 2018. Parkinson's disease: alpha synuclein, heme oxygenase and biotherapeutic countermeasures. Curr. Pharm. Des. 24, 2317–2321.
Hara, T., Takamura, A., Kishi, C., Iemura, S., Natsume, T., Guan, J.L., Mizushima, N., 2008. FIP200, a ULK-interacting protein, is required for autophagosome formation in mammalian cells. J. Cell Biol. 181, 497–510.
He, C., Levine, B., 2010. The beclin 1 interactome. Curr. Opin. Cell Biol. 22, 140–149.
Hosokawa, N., Hara, T., Kaizuka, T., Kishi, C., Takamura, A., Miura, Y., Iemura, S., Natsume, T., Takehana, K., Yamada, N., Guan, J.L., Oshiro, N., Mizushima, N., 2009. Nutrient-dependent mTORC1 association with the ULK1-Atg13-FIP200 complex required for autophagy. Mol. Biol. Cell 20, 1981–1991.
Jaber, N., Dou, Z., Chen, J.-S., Catanzaro, J., Jiang, Y.-P., Ballou, L.M., Selinger, E., Ouyang, X., Lin, R.Z., Zhang, J., 2012. Class III PI3K Vps34 plays an essential role in autophagy and in heart and liver function. Proc. Natl. Acad. Sci. 109, 2003–2008.
Jensen, P.S., Bak, J., 2002. Near-infrared transmission spectroscopy of aqueous solutions: influence of optical path length on signal-to-noise ratio. Appl. Spectrosc. 56, 1600–1606.
Jensen, J.L., Indurthi, V.S., Neau, D.B., Vetter, S.W., Colbert, C.L., 2015. Structural insights into the binding of the human receptor for advanced glycation end products (RAGE) by S100B, as revealed by an S100B-RAGE-derived peptide complex. Acta Crystallogr. D Biol. Crystallogr. 71, 1176–1183.
Jiang, X., Wang, X., Tuo, M., Ma, J., Xie, A., 2018. RAGE and its emerging role in the pathogenesis of Parkinson's disease. Neurosci. Lett. 672, 65–69.
Josephs, S., Henry, B., Balachandran, N., Strayer, D., Peterson, D., Komaroff, A., Ablashi, D., 1991. HHV-6 reactivation in chronic fatigue syndrome. Lancet 337, 1346–1347.
Komatsu, M., Waguri, S., Chiba, T., Murata, S., Iwata, J., Tanida, I., Ueno, T., Koike, M., Uchiyama, Y., Kominami, E., Tanaka, K., 2006. Loss of autophagy in the central nervous system causes neurodegeneration in mice. Nature 441, 880–884.
Kragh, C.L., Ubhi, K., Wyss-Corey, T., Masliah, E., 2012. Autophagy in dementias. Brain pathology 22, 99–109.
Lane, J.D., Korolchuk, V.I., Murray, J.T., Karabiyik, C., Lee, M.J., Rubinsztein, D.C., 2017. Autophagy impairment in Parkinson's disease. Essays Biochem. 61, 711–720.
Li, H., Qiu, S., Li, X., Li, M., Peng, Y., 2015. Autophagy biomarkers in CSF correlates with infarct size, clinical severity and neurological outcome in AIS patients. J. Transl. Med. 13, 359.
Liu, C., Gao, Y., Barrett, J., Hu, B., 2010. Autophagy and protein aggregation after brain ischemia. J. Neurochem. 115, 68–78.
Lorincz, P., Juhasz, G., 2020. Autophagosome-lysosome fusion. J. Mol. Biol. 432, 2462–2482.
Luo, T., Park, Y., Sun, X., Liu, C., Hu, B., 2013. Protein misfolding, aggregation, and autophagy after brain ischemia. Transl. Stroke Res. 4, 581–588.
Magalhães, S., Trindade, D., Martins, T., Rosa, I.M., Delgadillo, I., Goodfellow, B.J., Silva, O.A.D.C., Henriques, A.G., Nunes, A., 2020. Monitoring plasma protein aggregation during aging using conformation-specific antibodies and FTIR spectroscopy. Clinica Chimica Acta 502, 25–33.
Mandarano, A.H., Maya, J., Giloteaux, L., Peterson, D.L., Maynard, M., Gottschalk, C.G., Hanson, M.R., 2020. Myalgic encephalomyelitis/chronic fatigue syndrome patients exhibit altered T cell metabolism and cytokine associations. J. Clin. Invest. 130, 1491–1505.
Mathew, R., Karantza-Wadsworth, V., White, E., 2007. Role of autophagy in cancer. Nat. Rev. Cancer 7, 961–967.
Medow, M.S., Aggarwal, A., Baugham, I., Messer, Z., Stewart, J.M., 2013. Modulation of the axon-reflex response to local heat by reactive oxygen species in subjects with chronic fatigue syndrome. J. Appl. Physiol. 1985 (114), 45–51.
Meikle, P.J., Brooks, D.A., Ravenscroft, E.M., Yan, M., Williams, R.E., Jaunzems, A.E., Chataway, T.K., Karageorgos, L.E., Davey, R.C., Boulter, C.D., Carlsson, S.R., Hopwood, J.J., 1997. Diagnosis of lysosomal storage disorders: evaluation of lysosome-associated membrane protein LAMP-1 as a diagnostic marker. Clin. Chem. 43, 1325–1335.
Meng, F., Marek, P., Potter, K.J., Verchere, C.B., Raleigh, D.P., 2008. Rifampicin does not prevent amyloid fibril formation by human islet amyloid polypeptide but does inhibit fibril thioflavin-T interactions: implications for mechanistic studies of β-cell death. Biochemistry 47, 6016–6024.
Mensah, F.K.F., Bansal, A.S., Ford, B., Cambridge, G., 2017. Chronic fatigue syndrome and the immune system: where are we now? Neurophysiol. Clin. 47, 131–138.
Milivojevic, M., Che, X., Bateman, L., Cheng, A., Garcia, B.A., Hornig, M., Huber, M., Klimas, N.G., Lee, B., Lee, H., 2020. Plasma proteomic profiling suggests an association between antigen driven clonal B cell expansion and ME/CFS. PloS one 15, e0236148.
Mizushima, N., 2007. Autophagy: process and function. Genes Dev. 21, 2861–2873.
Mizushima, N., 2020. The ATG conjugation systems in autophagy. Curr. Opin. Cell Biol. 63, 1–10.
Mocellin, S., Bronte, V., Nitti, D., 2007. Nitric oxide, a double edged sword in cancer biology: searching for therapeutic opportunities. Med. Res. Rev. 27, 317–352.
Modi, K.K., Roy, A., Brahmachari, S., Rangasamy, S.B., Pahan, K., 2015. Cinnamon and its metabolite sodium benzoate attenuate the activation of p21rac and protect memory and learning in an animal model of Alzheimer's disease. PloS one 10, e0130398.
Morris, G., Maes, M., 2014. Mitochondrial dysfunctions in myalgic encephalomyelitis/chronic fatigue syndrome explained by activated immuno-inflammatory, oxidative and nitrosative stress pathways. Metab. Brain Dis. 29, 19–36.
Mort, J.S., Buttle, D.J., 1997. Cathepsin b. Int. J. Biochem. Cell Biol. 29, 715–720.
Moscat, J., Diaz-Meco, M.T., 2009. p62 at the crossroads of autophagy, apoptosis, and cancer. Cell 137, 1001–1004.
Motsenbocker, M., 1988. Sensitivity limitations encountered in enhanced horseradish peroxidase catalysed chemiluminescence. J. Biolumin. Chemilumin. 2, 9–16.
Nassif, M., Hetz, C., 2012. Autophagy impairment: a crossroad between neurodegeneration and tauopathies. BMC Biol. 10, 1–4.
Noda, N.N., Fujioka, Y., 2015. Atg1 family kinases in autophagy initiation. Cell. Mol. Life Sci. 72, 3083–3096.
Okamoto, K., Kondo-Okamoto, N., 2012. Mitochondria and autophagy: critical interplay between the two homeostats. Biochim. Biophys. Acta Gen. Subj. 1820, 595–600.
Osuka, K., Watanabe, Y., Takagi, T., Usuda, N., Atsuzawa, K., Yoshida, J., Takayasu, M., 2008. Activation of endothelial nitric oxide synthase following spinal cord injury in mice. Neurosci. Lett. 436, 265–268.
Puente, C., Hendrickson, R.C., Jiang, X., 2016. Nutrient-regulated phosphorylation of ATG13 inhibits starvation-induced autophagy. J. Biol. Chem. 291, 6026–6035.
Rabinowitz, J.D., White, E., 2010. Autophagy and metabolism. Science 330, 1344–1348.
Ranieri, E., Gerace, R.L., Ravenscroft, E.M., Hopwood, J.J., Meikle, P.J., 1999. Pilot neonatal screening program for lysosomal storage disorders, using lamp-1. Southeast Asian J. Trop. Med. Public Health 30 (Suppl. 2), 111–113.
Rasa, S., Nora-Krukle, Z., Henning, N., Eliassen, E., Shikova, E., Harrer, T., Scheibenbogen, C., Murovska, M., Prusty, B.K., <collab>European Network on, M. C</collab>, 2018. Chronic viral infections in myalgic encephalomyelitis/chronic fatigue syndrome (ME/CFS). J. Transl Med 16, 268.
Repnik, U., Stoka, V., Turk, V., Turk, B., 2012. Lysosomes and lysosomal cathepsins in cell death. Biochim. Biophys. Acta 1824, 22–33.
Roy, A., 2016. Targeting BPOZ-2 in lewy body disease. Neural Regen. Res. 11, 910–911.
Roy, A., Pahan, K., 2013. Ankyrin repeat and BTB/POZ domain containing protein-2 inhibits the aggregation of alpha-synuclein: implications for Parkinson's disease. FEBS Lett. 587, 3567–3574.
Roy, A., Fung, Y.K., Liu, X., Pahan, K., 2006. Up-regulation of microglial CD11b expression by nitric oxide. J. Biol. Chem. 281, 14971–14980.
Roy, A., Jana, A., Yatish, K., Freidt, M.B., Fung, Y.K., Martinson, J.A., Pahan, K., 2008. Reactive oxygen species up-regulate CD11b in microglia via nitric oxide: implications for neurodegenerative diseases. Free Radic. Biol. Med. 45, 686–699.
Roy, A., Ghosh, A., Jana, A., Liu, X., Brahmachari, S., Gendelman, H.E., Pahan, K., 2012. Sodium phenylbutyrate controls neuroinflammatory and antioxidant activities and protects dopaminergic neurons in mouse models of Parkinson's disease. PloS one 7, e38113.
Roy, A., Rangasamy, S.B., Kundu, M., Pahan, K., 2016. BPOZ-2 gene delivery ameliorates alpha-synucleinopathy in A53T transgenic mouse model of Parkinson's disease. Sci. Rep. 6, 1–14.
Saftig, P., 2006. Physiology of the lysosome. In: Fabry Disease: Perspectives From 5 Years of FOS.
Sharma, S., 2018. Autophagy-based diagnosis of pregnancy hypertension and pre-eclampsia. Am. J. Pathol. 188, 2457–2460.
Silvestre, I.B., Dagda, R.Y., Dagda, R.K., Darley-Usmar, V., 2019. Mitochondrial alterations in NK lymphocytes from ME/CFS patients. J. Immunol. 202, 126.139-126.139.

Streit, W.J., Xue, Q.S., 2016. Microglia in dementia with lewy bodies. Brain Behav. Immun. 55, 191–201.
Sun, H.J., Xiong, S.P., Wu, Z.Y., Cao, L., Zhu, M.Y., Moore, P.K., Bian, J.S., 2020. Induction of caveolin-3/eNOS complex by nitroxyl (HNO) ameliorates diabetic cardiomyopathy. Redox Biol. 32, 101493.
Surendranathan, A., Su, L., Mak, E., Passamonti, L., Hong, Y.T., Arnold, R., Vázquez Rodríguez, P., Bevan-Jones, W.R., Brain, S.A.E., Fryer, T.D., Aigbirhio, F.I., Rowe, J. B., O'Brien, J.T., 2018. Early microglial activation and peripheral inflammation in dementia with lewy bodies. Brain 141, 3415–3427.
Tanida, I., Ueno, T., Kominami, E., 2008. LC3 and autophagy. In: Autophagosome and Phagosome. Springer, pp. 77–88.
Tomas, C., Elson, J.L., Strassheim, V., Newton, J.L., Walker, M., 2020. The effect of myalgic encephalomyelitis/chronic fatigue syndrome (ME/CFS) severity on cellular bioenergetic function. PloS one 15, e0231136.
White, E., 2012. Deconvoluting the context-dependent role for autophagy in cancer. Nat. Rev. Cancer 12, 401–410.
Wirth, K.J., Scheibenbogen, C., 2021. Pathophysiology of skeletal muscle disturbances in myalgic encephalomyelitis/chronic fatigue syndrome (ME/CFS). J. Transl. Med. 19, 1–16.
Xie, J., Reverdatto, S., Frolov, A., Hoffmann, R., Burz, D.S., Shekhtman, A., 2008. Structural basis for pattern recognition by the receptor for advanced glycation end products (RAGE). J. Biol. Chem. 283, 27255–27269.
Xu, J., Xia, L., Shang, Q., Du, J., Zhu, D., Wang, Y., Bi, D., Song, J., Ma, C., Gao, C., Zhang, X., Sun, Y., Zhu, L., Wang, X., Zhu, C., Xing, Q., 2017. A variant of the autophagy-related 5 gene is associated with child cerebral palsy. Front. Cell. Neurosci. 11, 407.
Yuste, J.E., Tarragon, E., Campuzano, C.M., Ros-Bernal, F., 2015. Implications of glial nitric oxide in neurodegenerative diseases. Frontiers in Cellular Neuroscience 9.
Zachari, M., Ganley, I.G., 2017. The mammalian ULK1 complex and autophagy initiation. Essays Biochem. 61, 585–596.
Zhang, Z., Yue, P., Lu, T., Wang, Y., Wei, Y., Wei, X., 2021. Role of lysosomes in physiological activities, diseases, and therapy. J. Hematol. Oncol. 14, 79.
Zhao, P., Zhu, Y., Sun, L., Zhu, W., Lu, Y., Zhang, J., Mao, Y., Chen, Q., Zhang, F., 2021. Circulating exosomal miR-1-3p from rats with myocardial infarction plays a protective effect on contrast-induced nephropathy via targeting ATG13 and activating the AKT signaling pathway. Int. J. Biol. Sci. 17, 972–985.